Coordination Chemistry Reviews 362 (2018) 1–23

Contents lists available at ScienceDirect

Coordination Chemistry Reviews

journal homepage: www.elsevier.com/locate/ccr

Review

Metal–organic framework-derived porous materials for catalysis

Yu-Zhen Chen [a,b,1], Rui Zhang [a,1], Long Jiao [a], Hai-Long Jiang [a,*]

[a] Hefei National Laboratory for Physical Sciences at the Microscale, CAS Key Laboratory of Soft Matter Chemistry, Collaborative Innovation Center of Suzhou Nano Science and Technology, Department of Chemistry, University of Science and Technology of China, Hefei, Anhui 230026, PR China
[b] College of Chemistry and Chemical Engineering, Qingdao University, Qingdao, Shandong 266071, PR China

ARTICLE INFO

Article history:
Received 12 January 2018
Accepted 12 February 2018

Keywords:
Metal–organic frameworks
Porous materials
Derivatives
Catalysis

ABSTRACT

Metal–organic frameworks (MOFs), constructed by metal ions/clusters and organic linkers, featuring crystalline porous structures, have been intensively employed as templates/precursors for the synthesis of diverse porous materials including porous carbons, metal-based compounds (such as metal oxides/carbides/phosphides) and their composites. The large surface area, high porosity and excellent tailorability of MOFs can be well inherited to their derivatives, making MOF-derived porous materials very promising for catalytic applications. Herein, we systematically summarize the versatile synthetic strategies to fabricate MOF-derived porous materials and give an overview on their recent progress on organic heterogeneous catalysis, photocatalysis and electrocatalysis. Finally, the challenges and prospects related to MOF-derived porous materials for catalysis are also discussed.

Contents

Abbreviations: BDC, 1,4-benzenedicarboxylate; BTC, benzenetricarboxylate; NDC, 1,4-naphthalenedicarboxylate; TPT, 2,4,6-tris(4-pyridyl)-1,3,5-triazine; MeIM, 2-methylimidazole; DOBDC, 2,5-dihydroxyterephthalate; TCPP, tetrakis(4-carboxyphenyl)porphyrin; H_2bpydc, 2,2′-bipyridine-5,5′-dicarboxylic acid; Ted, triethylenediamine; FA, fumaric acid; MOF-5, $Zn_4O(BDC)_3$; MOF-253, Al(OH)(bpydc); HKUST-1, $Cu_3(BTC)_2$; NENU-5, $[Cu_2(BTC)_{4/3}(H_2O)_2]_6[H_3PMo_{12}O_{40}]$; ZIF-8, $Zn(MeIM)_2$; ZIF-67, $Co(MeIM)_2$; Co^{II}MOF, $Co_9(btc)_6(tpt)_2(H_2O)_{15}$; UiO-66–$NH_2$, $Zr_6O_4(OH)_4(BDC–NH_2)_6$; PCN-224, $Zr_6O_4(OH)_8(TCPP)_2$; PCN-224(Zn), $Zr_6O_4(OH)_8(Zn\text{-}TCPP)_2$; M-MOF-74, $M_2(dobdc)(H_2O)_2\cdot 8H_2O$ M = Ni or Co; MIL-53, [M(OH)(BDC)]*n*, M = Al or Fe; Fe–MIL-88A, $Fe_3O(FA)_3\text{-}(H_2O)_2(NO_3)$; Fe–MIL-88B, $Fe_3O(BDC)_3\text{–}(H_2O)_2(NO_3)$; MIL-88B–$NH_2$, $Fe_3O(H_2N–BDC)_3$; Fe–MIL-101, $[Fe_3F(H_2O)_2O(BDC)_3]nH_2O$, $n \sim 25$; Ti–MIL-125, $Ti_8O_8(OH)_4(BDC)_6$; Ni–MOF, $Ni_3(BTC)_2\cdot 12H_2O$; Co–PBA, $Co_3[Co(CN)_6]_2$; MAF-6, RHO-$[Zn(eim)_2]$ (Heim = 2-ethylimidazole); Al–PCP, Al(OH)(1,4-NDC)·$2H_2O$; F–T synthesis, Fischer–Tropsch synthesis; FTY, mol of CO converted to hydrocarbons per gram of Fe per second; QD, quantum dot; PBA, Prussian blue analog (PBA); NF, nickel foam; GO, graphene oxide; rGO/RGO, reduced graphene oxide; NPs, nano particles; NPC, N-doped porous carbon; M, metal; MO, metal oxide; MC, metal carbide; MS, metal sulfide; MP, metal phosphide; TOF, turnover frequency; ORR, oxygen reduction reaction; OER, oxygen evolution reaction; HER, hydrogen evolution reaction; CO_2RR, CO_2 reduction reaction; MOR, methanol oxidation reaction; XRD, X-ray diffraction; XAFS, X-ray absorption fine structure spectroscopy; DRIFTS, diffuse reflectance infrared Fourier transform spectroscopy; FTIR, Fourier transform infrared spectroscopy.

* Corresponding author.
E-mail address: jianglab@ustc.edu.cn (H.-L. Jiang).
[1] These authors contributed equally to this work.

https://doi.org/10.1016/j.ccr.2018.02.008
0010-8545/

1. Introduction

Nanoporous materials, such as the classical zeolites and mesoporous silica, have been intensively investigated as ideal platforms for various applications, including gas storage, chemical sensing, energy conversion, catalysis, etc [1–7]. Particularly, due to the high surface area and confined pore space that can be functionalized, nanoporous materials have demonstrated great superiority. For instance, zeolites, constructed by micropores in the range of 0.3–1.5 nm, have excellent gas adsorption capability. Moreover, zeolites are able to differentiate molecules with different sizes, which is of vital significance in selective catalysis. These merits, along with the stability, contribute to the important applications of zeolites in petrochemical industry and synthesis of fine chemicals [8,9]. As for mesoporous silica with larger pore sizes, the applications are mostly focused on drugs delivery, energy conversion and storage, as well as catalysis, thanks to their uniform mesopores, moderate surface area, good biocompatibility and ability to interact with guest species [10–13]. Given the pore size gap between microporous zeolites and mesoporous silica, it is important to find alternative materials possessing ordered pore structures to bridge the above gap.

Metal–organic frameworks (MOFs), also known as porous coordination polymers (PCPs), featuring well defined pores with diameters ranging from 0 (nonporous) to 9.8 nm, have been proven to be outstanding candidates for bridging the gap between zeolites and mesoporous silica. They have achieved rapid development over the past two decades for diverse applications, such as gas sorption/separation [14–16], catalysis [17–28], chemical sensing [29–31], energy storage and conversion [32–34], etc. Featuring well-defined crystalline structures, adjustable pore topology, ultrahigh surface areas and excellent tailorability, MOFs have shown huge potential especially in catalysis [35–38]. However, due to the fragile coordination bonding between metal nodes and organic ligands, the instability, especially moisture sensitivity [39], limits the practical applications of MOFs. Taking photocatalytic water splitting as an example, the reaction environment (aqueous solutions) and the existence of sacrificial agent may exert a negative influence on the stability of MOFs [40]. Moreover, in electrocatalytic reactions, the low electrical conductivity further impedes the application of pristine MOFs and very limited related studies were reported [41,42]. The good thing is that, when served as templates/precursors, MOFs can be converted to much more stable and conductive carbon/metal-based porous materials than pristine MOFs, with inherited characters of pristine MOFs to a large degree, such as large surface area, composition diversity and dispersion, tailored porosity [43–49]. In addition, considering that most MOFs are constructed by transition metals (Mn, Fe, Co, Ni, Cu, etc.) and organic ligands containing C, H, O, N, S, etc., which are usually necessary elements in catalytic systems, the derivatives with the same elementary compositions as parent MOFs would possess great potentials in catalysis [50–59]. In addition, compared with traditional catalysts, the MOF-derived porous materials have more advantages, such as large surface area, high porosity, adjustable morphology and uniform heteroatom doping, which are considered to be crucial to their catalysis. Therefore, many MOF-derived porous materials even afford better performances than their parent MOFs.

As a matter of fact, the derivation of MOFs opens up an avenue to the preparation of diversified porous materials with unique advantages in comparison to traditional nanoporous materials, mainly on the following points: (i) simple and convenient synthetic procedures without additional templates (providing a simple method to fabricate porous materials); (ii) ordered porous structure and easy adjustment of pore size (guaranteeing high-flux mass transfer and easy accessibility of active sites); (iii) high surface area (exposure of high-density active sites); (iv) controllable size and inherited morphology of pristine MOFs (benefitting the optimization of catalytic performance); (v) facile doping of highly dispersed heteroatoms (modulating the local electronic structure of catalysts); (vi) accurate control of active sites through the predesign of MOF precursors (favoring the establishment of structure–performance relationship). Therefore, MOF-derived porous materials, with large surface area, high stability and tunable structures, are very promising candidates for catalysis [50–61].

In this review, we present a systematic introduction of derivation strategies of MOFs to porous materials at first. Then an overview on the recent progress of MOF-derived nanomaterials for various catalytic applications is summarized. For heterogeneous catalysis, MOF-derived porous materials have great potential in rational loading of active sites and functionalization with heteroatoms, which is critical for reactions such as oxidation, reduction and CO_2 fixation. Moreover, many metal-based compounds, such as metal oxides, metal sulfides and others derived from MOFs are semiconductors, which are favorable for photocatalysis. The porosity of MOF-based porous materials creates the opportunity for rapid consumption of photo-induced charge carriers, resulting in improved photocatalytic efficiency. In terms of electrocatalysis, the large surface area, appropriate pore sizes as well as conductivity in the porous materials derived from MOFs are closely related to the performance of electrocatalysts. Finally, particular challenges as well as research opportunities of porous materials derived from MOFs for further development toward catalysis are also critically discussed.

2. Fabrication strategies for MOF-derived porous materials

Given the diversified compositions and tailorable structures, the derivation of MOFs has been considered as an alternative choice for the fabrication of porous materials. Generally, the preparation of MOF-derived porous materials, including carbons, metal-based compounds (e.g., metal phosphide/oxides/carbides/sulfides) and their hybrids [43–65], mainly relies on a facile pyrolysis under a certain atmosphere (e.g., Ar, N_2, air) or a simple solution infiltration method followed by heat treatment (Scheme 1). The pore sizes, morphologies, compositions, as well as properties of MOF-derived materials can be partially inherited from MOF precursors and tuned to some extent, through the rational design of the MOF precursors and extrinsic control of the synthetic procedures (e.g., gas atmosphere, annealing temperature/time, heating rate and the amount of the precursor). Based on the experimental conditions and interaction between MOFs and related objects, the synthetic strategies of MOF-derived materials can be generally divided into four types.

2.1. Direct pyrolysis of MOFs

This method provides a simple yet effective way to various porous materials via a direct pyrolysis of MOF precursors. For the preparation of metal-free carbons, the MOF precursors are generally carbonized under inert (such as Ar, N_2) atmosphere with *in situ* evaporation or/and subsequent leaching of metal species. As a very early-stage report, Jiang et al. obtained porous carbons by direct pyrolyzing ZIF-8 to give porous carbon with surface area as high as 3067 $m^2 g^{-1}$ [66]. It was found that the introduction and polymerization of furfuryl alcohol into ZIF-8 further improved the surface area of porous carbons (3405 $m^2 g^{-1}$). Right after this, Hu et al. synthesized nanoporous carbons with an even higher surface area (5500 $m^2 g^{-1}$) via the simple pyrolysis of Al–PCP and subsequent removal of Al species [67]. It is noteworthy that the resultant carbons doped with heteroatoms (N, P, S, etc.) are generally obtained through the direct pyrolysis of MOFs with heteroatom-involved organic ligands or/and the linkers with functional groups ($-NH_2$, $-SO_3H$, etc.).

Aside from porous carbons, many porous MO nanostructures, including cobalt oxide (Co_3O_4) [68,69], titanium dioxide (TiO_2) [70], iron oxides (Fe_xO_y) [71], zinc or copper based oxides (ZnO, CuO_x) [72], have also been successfully synthesized from MOFs with (partially) preserved morphology, usually through pyrolysis under air or oxygen to remove carbons. As a very early-stage study, Liu et al. prepared agglomerated Co_3O_4 nanoparticles (NPs) with a diameter of about 250 nm through the direct pyrolysis of cobalt–MOF ($Co_3(NDC)_3(DMF)_4$) at 600 °C for 1 h under air [68]. The agglomerated structure made up of smaller Co_3O_4 NPs (25 nm) is favorable to enhance the performance of lithium ion batteries. Khaletskaya et al. synthesized gold NPs loaded on the surface of porous TiO_2 (GNP/TiO_2) by pyrolysis of GNP/NH_2–MIL-125(Ti) for 2 h under O_2 atmosphere [70]. Similarly, porous Co_3O_4 are commonly derived from various Co-based MOFs such as ZIF-67 [69], Co-Prussian blue analogs (PBA) ($Co_3[Co(CN)_6]_2$) [73] and MOF-71 [74]. Salunkhe et al. obtained porous Co_3O_4 polyhedra by treating ZIF-67 as a precursor [69]. ZIF-67 was first pyrolyzed at 500 °C for 30 min under N_2 atmosphere, which effectively impeded the collapse of the structure and retained the morphology of MOF precursors. Then the cooled sample was treated at 350 °C for 2 h in air for the preparation of Co_3O_4 polyhedra. The Fe-based MOF, MIL-88, was utilized as a precursor to give mesoporous spindle-like Fe_2O_3 with small sizes of *ca.* 20 nm [75].

Two or more component-involved hybrid structures, typically carbon-supported metal/metal oxides and hybrids of various metal-based compounds, can be readily obtained. The hybrid structures are prepared through the direct carbonization of MOFs under inert atmosphere, similar to the fabrication of porous carbons, just without the removal of metal species. For example, anthill-like Cu@C hybrid materials have been prepared from the pyrolysis of HKUST-1 under N_2 atmosphere, with retained octahedral morphology for electrocatalytic oxidation of glucose [76]. The performance of the catalysts is closely bound up with the Cu particle size and the surface area, which can be controlled by the temperature and time length of pyrolysis. By a direct annealing of ZIF-8 analog (Cu–Co–ZIF) at 500 °C for 2 h under argon atmosphere, porous carbon-coated $CuCo_2O_4$ concave polyhedra ($CuCo_2O_4$/C) were successfully synthesized, which presented excellent performance as anode materials of lithium-ion batteries [77].

2.2. Pyrolysis of MOFs encapsulating guest species

The incorporation of guest species into MOF pores can serve as a flexible and effective strategy and this is very popular toward the fabrication of MOF-derived porous materials [78–88]. Considering that direct pyrolysis of MOFs might give limited active sites, the

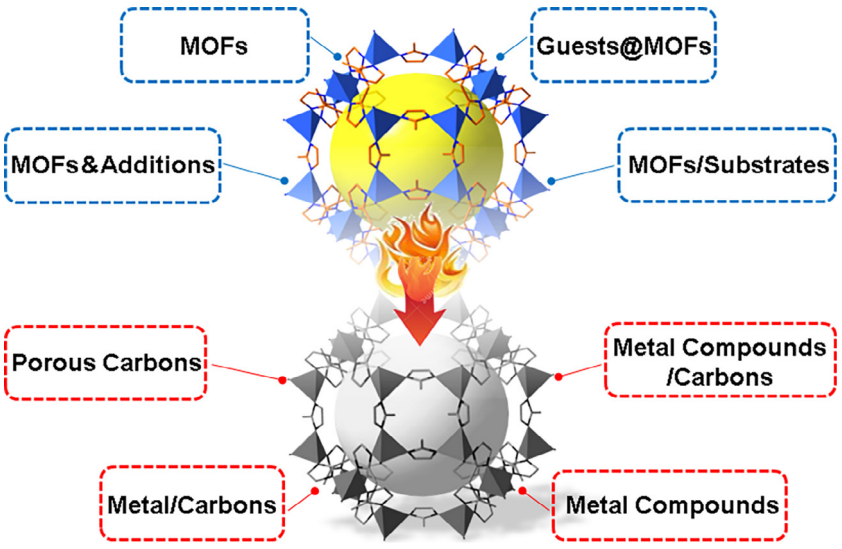

Scheme 1. Illustration showing the fabrication of diverse porous materials from MOFs and MOF-based composites as templates/precursors via pyrolysis.

rational introduction of guest species into MOFs followed by pyrolysis affords great opportunity to fabricate target porous catalysts with desired compositions, which are promising in many fields, especially electrocatalysis [83]. As a seminal study, Xu's group demonstrated MOF-5 as a suitable precursor/template to incorporate furfuryl alcohol for preparing porous carbons with high surface area (2872 $m^2 g^{-1}$) [78]. During the pyrolysis of MOF-5 under inert atmosphere, the generated ZnO species was reduced by carbon to produce evaporative Zn at high temperature (>700 °C), yielding highly porous carbon. Xu and co-workers also reported N-doped nanoporous carbons with large Brunauer–Emmett–Teller (BET) surface area and high N contents through the pyrolysis of ZIF-8 filled with furfuryl alcohol and NH_4OH, which exhibited excellent selectivity toward CO_2 uptake and two-electron process in oxygen reduction reaction (ORR) [84]. Using the NENU-5 inserted with Mo-based polyoxometalates (POMs) ($H_3PMo_{12}O_{40}$) as precursor, Lou and co-workers prepared ultrafine molybdenum carbide NPs (MoC_x nanooctahedra) [85]. Similarly, Fe-containing complexes like iron(III)acetylacetonate ($Fe(acac)_3$) and ammonium ferric citrate were also introduced to the pores of ZIF-8 for the construction of iron–nitrogen active sites for electrocatalytic ORR [83,86].

2.3. Pyrolysis of MOFs composited with various substrates

To fabricate different porous materials for targeted applications, quite a few MOFs as building blocks have been assembled onto various substrates, such as graphene oxide (GO), Ni foam (NF), carbon cloth, etc. Given the electrocatalytic process requires good electronic conductivity for the catalyst, these substrates with high conductivity greatly improve charge transfer at the interface between the electrolyte and active compositions, which can be derived from the pyrolysis of MOF assemblies. Furthermore, the substrates benefit the stabilization of active species and enable their good dispersion, which are favorable to the efficiency and recyclability of the catalysts [89]. Considering that GO could effectively realize the consecutive electronic conductivity, Zhong et al. prepared the N-doped porous carbon-coated GO hybrids via the pyrolysis of the ZIF-8/GO composite, exhibiting excellent electrocatalytic activity for ORR [90]. Zhang et al. successfully synthesized ZnO nanorod@ZnO QD–carbon hybrid with a core–shell structure by thermal treatment of the ZIF-8-coated ZnO nanorod [91]. Recently, Jiao et al. prepared CoP/reduced graphene oxide (rGO) composite through the pyrolysis of ZIF-67/GO and subsequent phosphorization [92].

Not limited to the random MOF growth, MOF nanoarrays assembled on substrates have also been fabricated to give MOF-derived porous material arrays attached on the substrates via pyrolysis. Under the circumstances of electrocatalysis over resultant nanoarrays, the substrates usually behave as current collectors. On the one hand, the open space of MOF-derived nanoarrays will contribute to the fast diffusion of electrolytes and greatly enhance the accessibility of the active sites. On the other hand, the close contact between the current collectors and the nanoarrays ensures fast charge transfer. Furthermore, these structures usually possess excellent mechanical strength, which is favorable for the stability of the catalysts [93]. A case in point is the pyrolysis of Co-based MOF (Co–naphthalenedicarboxylate MOF) arrays to hybrid porous Co_3O_4/C nanowire arrays supported on Cu foil, which exhibit excellent activity and stability for electrocatalysis [93]. Cai et al. develop a general strategy for the preparation of metal oxide@MOF-derived porous carbon hybrid arrays through the pyrolysis of metal oxide@MOF or metal hydroxide@MOF hybrid arrays grown on various substrates for efficient electrocatalysis more recently [94].

2.4. Solution infiltration method followed by heat treatment

In addition to the pyrolysis approach mentioned above, the infiltration of MOFs in the solution with particular precursors followed by moderate heat treatment is able to afford porous metal-based compounds such as metal sulfides, with original MOF shape maintained to some extent. This synthetic route, under relatively low/moderate temperatures, enriches the fabrication strategies of MOF-derived porous materials. Recently, MOFs as precursors have been intensively used to generate porous metal sulfide nanostructures, generally through sulfidation with various sulfur sources (e.g., sodium sulfide, sulfur powder and thioacetamide) [95,96]. The subsequent heat treatment is vital for the conversion to metal sulfides. Without heat treatment, the synthesized metal sulfides tend to be amorphous, presenting powder X-ray diffraction (XRD) patterns in the absence of characteristic peaks [95]. Cho et al. have fabricated Cu–MOF (HKUST-1) with CuS NPs by introducing thioacetamide into the pores of HKUST-1 followed by heat treatment with different temperatures [97]. The conductivity of the obtained catalyst can be optimized by adjusting the sulfuration reaction time and the sulfur amount. Lou's group have prepared NiS hollow nanoframes with tunable size and cubic shape inherited from the PBA precursor based on the reaction between PBA and Na_2S [95]. Similarly, ZnS nanocages with an average size of 400 nm were successfully obtained by refluxing the ZIF-8 precursor and thioacetamide (sulfur precursor) [98].

3. MOF-derived porous materials for heterogeneous catalysis

Recent reports have demonstrated that MOFs are ideal precursors for the construction of heterogeneous catalysts [99–157], such as porous carbons [125,126,130], metal/metal oxide/metal sulfide/metal phosphide nanostructures [118,119,136–142,157] and their composites [99–117,120–124,131,143,147–151,156] for various organic reactions. The MOF-derived porous materials possess their special advantages in these reactions. The catalytically active elements involved in MOF precursors can be inherited to their derived materials, while the stability of the derived catalysts is greatly improved compared with the original MOFs. Meanwhile, the metal clusters coordinated by organic linkers might effectively prohibit the agglomeration of resultant metal NPs to some extent during pyrolysis. Moreover, the high surface area and large porosity ensure the accessibility of active sites as well as the diffusion of substrates and products. In previous reports, the ZIF and MIL series, Cu–BTC and other Fe, Co, Ni, Cu-based MOFs or MOF-based composites are frequently utilized as templates/precursors for the preparation of porous materials toward heterogeneous catalysis, including liquid-phase organocatalysis and gas-phase catalysis (Table 1).

3.1. Liquid-phase organocatalysis

3.1.1. Oxidation reaction

In recent 3 years, a number of MOF-derived nanocomposites have been developed for various oxidation reactions, especially for oxidation of alcohols, oxidative coupling of amines and aerobic epoxidation of styrene [99–108]. To date, a series of Fe, Co or Ni-involved porous carbon catalysts have been synthesized by using these transition metal-based MOFs as precursors. Jiang's group designed a highly efficient and recyclable Co@CoO catalytic system by means of pyrolyzing ZIF-67 under N_2 atmosphere (Fig. 1a) [102]. Owing to the surface oxidation of Co NPs, the CoO and Co coexist in the catalyst. The optimized NC-700-3h catalyst exhibited excellent conversion and selectivity as well as recyclability toward the cross-esterifications of aromatic alcohols under very mild

Table 1
Summary of the MOF-derived porous materials and their catalytic heterogeneous reactions.

Catalyst	MOF precursor	Catalytic reaction	Refs.
C–N–Co	ZIF-67	Styrene epoxidation	[99]
Cu@C	Cu–BTC	TMB oxidation	[100]
Co@C–N	ZIF-67	Alcohol esterification	[101]
Co–CoO@NC	ZIF-67	Alcohol esterification	[102]
Co@C–N	Co^{II}MOF	Oxidative amidation of aldehyde	[103]
Fe_3O_4@C	MIL-88B	Alcohol oxidation	[104]
Fe–Co/C	MIL-45b	5-Hydroxymethylfurfural oxidation	[105]
Co/CN	ZIF-67	Cyclohexane, toluene oxidation; oxidative coupling of amines	[106]
Ru_3@CN	$Ru_3(CO)_{12}$@ZIF-8	Alcohol oxidation	[107]
Co@C–N	$Co_9(btc)_6(tpt)_2(H_2O)_{15}$	Alcohol oxidation	[108]
Pd/NPC–ZIF-8	ZIF-8	Biofuel upgrade	[109]
Ru SAs/N–C	UiO-66–NH_2	Quinoline hydrogenation	[110]
Pd@CN	ZIF-67	Phenol hydrogenation	[111]
Co@C–N	Co–MOF	Unsaturated bonds hydrogenation	[112]
Co@NC	[Co(TPA)(ted)$_{0.5}$]	α,β-Unsaturated aldehydes hydrogenation	[113]
Co–DABCO–TPA@C-800	Co–MOF	Reductive amination of aldehyde	[114]
Co@NC	ZIF-67	4-Nitrophenol reduction	[115]
N-doped Co@C	Co–MOF	Nitriles hydrogenation	[116]
Ni@C	$[Ni_3(OH)_2(C_8H_4O_4)_2(H_2O)_4]$	Nitro compounds hydrogenation	[117]
Ni/SiO_2	Ni–MOF/SiO_2	Benzene hydrogenation	[118]
Co_3S_4	ZIF-67	Nitroarenes hydrogenation	[119]
Co–Ni@C–N	Co–Ni–MOF	Benzonitrile hydrogenation	[120]
Co@Pd/NC	ZIF-67	Nitroarenes hydrogenation	[121]
PtCo@NHPC-1	ZIF-8	Nitro compounds hydrogenation	[122]
γ-Fe_2O_3@C	Fe–MIL-88A	Nitro compounds hydrogenation	[123]
Co–CoO@NC	ZIF-67	NH_3BH_3 dehydrogenation; nitro compounds hydrogenation	[124]
PCN-224–T	PCN-224	4-Nitrophenol reduction	[125]
Pd/Cz–MOF-253-800	MOF-253	Knoevenagel condensation–hydrogenation	[126]
C–ZIF-*n*	ZIF-7,8,9,67	CO_2 fixation	[130]
ZnO@NPC	ZIF-8	CO_2 fixation	[131]
CuO/CeO_2	Cu–BTC	CO oxidation	[136]
CeO_2:Cu^{2+}	Ce(Cu)–BTC	CO oxidation NO reduction	[137]
CuO/TiO_2	Cu–BTC/TiO_2	CO oxidation	[138]
CuO/Cu_2O	Cu–BTC	CO oxidation	[139]
Cu/CuO_X/C	Cu–BTC	CO oxidation	[140]
CeO_2–Co_3O_4	CeO_2–ZIF-67	NO reduction	[141]
CuO/CeO_2	Ce–UiO-66	CO oxidation	[142]
Co/C	ZIF-67	CO oxidation (low temperature)	[143]
Fe@C	Fe–BTC	Fischer–Tropsch	[147]
Fe@C	Fe–BTC	Fischer–Tropsch	[148]
Fe_3O_4@Fe_5C_2	Fe–MIL-88B/C	Fischer–Tropsch	[149]
Co@C	Co–MOF-74	Fischer–Tropsch	[150]
Fe/Na/S–C	Fe–BTC	Fischer–Tropsch	[151]
Cu/Zn@C	Zn–Cu–BTC	Water–gas shift	[156]
Ru/ZrO_2	Ru/UiO-66	CO_2 methanation	[157]

conditions (80 °C, 1 bar O_2), due to the specific structure and composition. The porous structure effectively promotes mass transport and protects the Co NPs from agglomeration. Other MOF-derived porous catalysts, such as Co@C–N [103], Fe_3O_4@C [104] and Fe–Co/C [105], have also been developed by simple pyrolysis of Co^{II}MOF (formulated $Co_9(btc)_6(tpt)_2(H_2O)_{15}$), MIL-88B and MIL-45b, respectively. In addition to the component design for the catalysts, the intrinsic structures also play a significant role in the performance of the catalysts. For example, the metal-free catalysts were prepared with pyrolysis of ZIF-67 under argon atmosphere and subsequent acid leaching (Fig. 1b) [106]. The obtained catalysts revealed good performance toward the aerobic oxidation of cyclohexane, toluene and oxidative coupling of amines to imines, which can be assigned to the specific electronic structures of graphitized N species existed in the carbon matrix. The electronegative N makes *ortho*-carbon prior positions adsorb O_2 molecules and generate peroxide species. The obtained peroxide species can be further stabilized by *ortho*-carbon, which is vital for the high selectivity. Bai et al. investigated the reactivity of oxidative amidation of aldehydes over Co NPs embedded in the N-doped porous carbons [103]. The Co^{II}MOF was utilized as a precursor for the preparation of a series of catalysts, with simple pyrolysis under argon atmosphere at different temperatures ranging from 500 °C to 900 °C. They discovered that the Co@C–N600 catalyst displayed the best performance for the oxidative amidation of aldehydes, compared with other counterparts treated with different temperatures.

Not limited to metal NPs, highly dispersed clusters can also be stabilized by MOF-derived porous carbons. Most recently, Li and co-workers successfully prepared uniform Ru_3 clusters stabilized by N species (Ru_3/CN) via pyrolysis of the composite, where $Ru_3(CO)_{12}$ is confined to the cavities of ZIF-8 [107]. Moreover, the Ru_3/CN catalyst revealed superior performance toward the oxidation of 2-aminobenzaldehyde with 100% conversion, 100% selectivity and a TOF of 4320 h^{-1}, far exceeding those of Ru particles and even single Ru atoms.

3.1.2. Reduction reaction

Various noble metals (e.g., Ru, Pt and Pd) have been widely applied in the hydrogenation reactions of many compounds including nitrocompounds, aldehydes, imines and ketones. The MOF-derived porous carbons are able to stabilize active noble metal NPs for these conversions. Jiang and co-workers reported ZIF-8 pyrolysis product, N-doped carbon, can be employed to

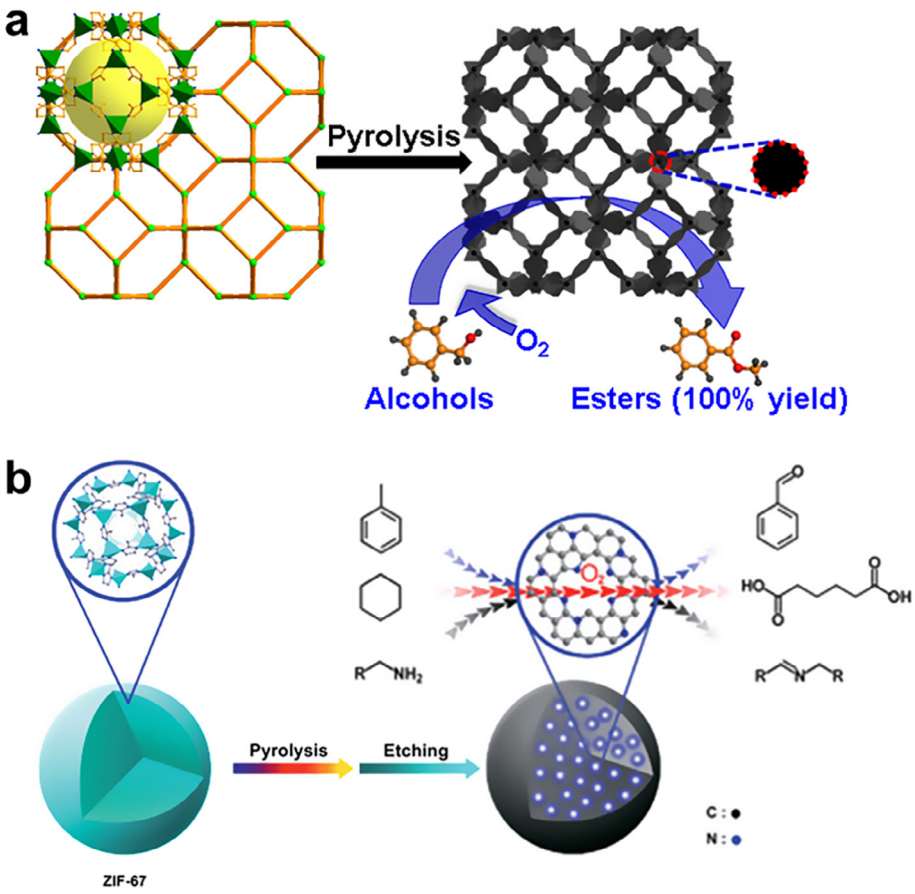

Fig. 1. (a) ZIF-67 derived Co@CoO for oxidation of alcohols to the corresponding esters. Adapted with the permission from Ref. [102]. Copyright 2015, The Royal Society of Chemistry. (b) Noble-metal-free catalyst (Co/CN) derived from pyrolysis-etching of ZIF-67 for aerobic oxidation of cyclohexane, toluene and oxidative coupling of amines to imines. Adapted with the permission from Ref. [106]. Copyright 2016, The Royal Society of Chemistry.

stabilize ultrafine Pd NPs for bio-oil refining, in which the good hydrophilicity of the catalyst plays a critical role [109]. The Pd/NPC–ZIF-8-900 completed the hydrodeoxygenation of vanillin and gave selectivity (80%) in 1 h with high TOF of 160 h^{-1}, surpassing all previous catalysts under identical conditions, which can be ascribed to the hydrophilicity, high content of graphitic-N, large surface area and ultrafine electron-rich Pd NPs in the catalyst.

Given the high cost of noble metals, the catalytic systems in transfer hydrogenation reactions have been extended to transition metal catalysts, including highly soluble and effective Co [112–116], Ni [117,118] based materials. The catalytic hydrogenation of various unsaturated bonds (C═C, C═N, C═O), benzene, phenol or nitroarenes over MOF-derived carbon composites have recently been studied [112–126]. Li and co-workers used Co-containing MOF ($[Co_9(btc)_6(tpt)_2(H_2O)_{15}]\cdot 2DMF\cdot 0.2H_2O$) as a precursor to develop a novel non-noble Co@C–N system, which was applied for catalytic hydrogenation of a variety of unsaturated bonds under mild conditions with excellent efficiency, flexibility and recyclability [112]. Recently, Liu et al. proposed a new strategy to synthesize Co@NC catalyst by using N-containing Co–MOF ($Co(TPA)(ted)_{0.5}$) for highly selective hydrogenation of α,β-unsaturated aldehydes under mild conditions [113]. Meanwhile, some porous composites, such as Ni@C [117] derived from Ni–MOF, have also been applied to catalyze hydrogenation reactions. Very recently, Beller and co-workers synthesized cobalt NPs encapsulated by a graphitic shell through the pyrolysis of MOF precursor (Co–DABCO–TPA) supported on carbon under argon atmosphere for 2 h (Fig. 2a) [114]. As a broadly effective reductive amination system, the catalyst is very efficient for the selective reductive amination of aldehydes to the corresponding primary amines with excellent yields. Even the reductive amination of ketones is slower than that of aldehydes, the catalyst can still bring its functions into full play. Not limited to the synthesis of primary amines, the catalyst also exhibits comparative activity for obtaining secondary and tertiary amines, which is of paramount importance for the preparation of drug molecules.

Apart from the utilization of monometallic NPs, Long et al. developed a facile approach to preparing transition-metal alloy NPs embedded in N-doped graphene from hetero-dinuclear MOFs [120]. Among all alloy NPs, the Co–Ni(3:1)@C–N exhibited remarkable activity for transfer hydrogenation of various substituted nitriles. Similarly, by choosing ZIF-67 as the precursor, Li and co-workers designed Co@Pd core–shell NPs embedded in the carbon matrix containing N species, (Co@Pd/NC) [121], which revealed good catalytic performance for hydrogenation of nitrobenzene with a conversion of 98%, surpassing that of most previous catalysts under similar reaction conditions.

In addition to the participation of metal NPs, the loading of metal oxide onto the carbon matrix can also be utilized for catalytic reduction reactions. Jiang's group used Fe-MIL-88A as a template for the preparation of γ-Fe_2O_3 NPs embedded in porous carbon, which exhibited outstanding catalytic hydrogenation performance for both aromatic and aliphatic nitro compounds to their amines [123]. Later, they synthesized Co–CoO@NC catalyst with ZIF-67 for effective tandem dehydrogenation of NH_3BH_3 and hydrogenation of nitro compounds at room temperature [124]. A variety of substituted aromatic or aliphatic nitro compounds were completely converted into their corresponding amines within

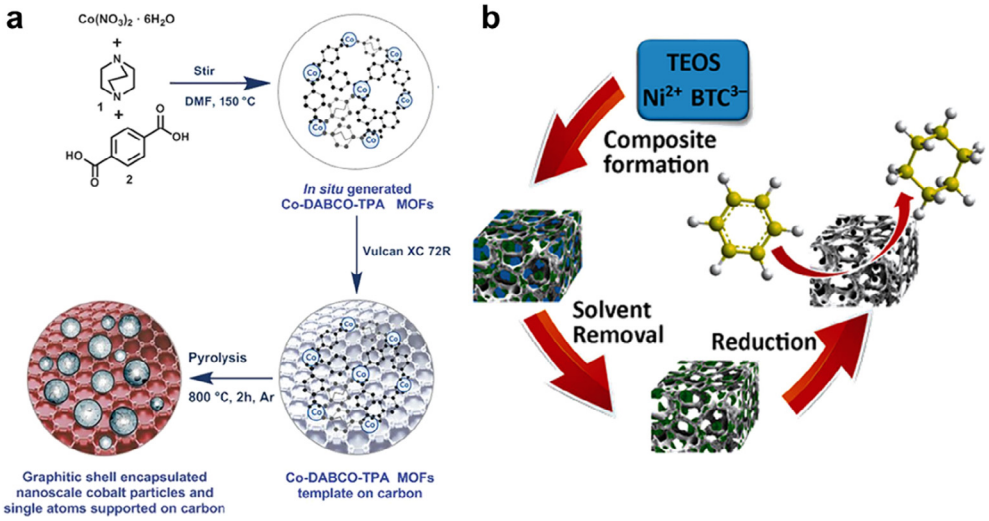

Fig. 2. (a) Schematic illustration of the synthesis of Co NPs supported on carbon. Adapted with the permission from Ref. [114]. Copyright 2017, American Association for the Advancement of Science. (b) Scheme of the preparation of Ni/SiO_2 catalysts and catalytic hydrogenation of benzene. Reproduced with the permission from Ref. [118]. Copyright 2016, Wiley-VCH.

several hours by taking advantage of *in situ* generated hydrogen from NH_3BH_3.

Aside from metal/metal oxide NPs embedded in the carbon matrix, some MOF-derived metal-free catalysts are active for catalytic hydrogenation as well. Huang et al. have developed three metal-free porous carbon materials, denoted as PCN-224-T, MOF-5-T and ZIF-8-T, via facile pyrolysis of their respective MOF precursors [125]. Amongst them, PCN-224-700 exhibited the best catalytic performance in the hydrogenation of 4-nitrophenol, which can be ascribed to high contents of pyrrolic nitrogen. Theoretical investigations indicated that pyrrolic nitrogen had a strong affinity toward 4-nitrophenol so that the nitro groups can get activated for the enhancement of the performance. Li et al. recently proposed a new MOF-template strategy for the synthesis of N-doped porous carbon (denoted as Cz–MOF-253) from MOF-253 containing 2,2′-bipyridyl [126]. The obtained Cz–MOF-253 exhibited excellent catalytic efficiency and cyclic stability in the Knoevenagel condensation reaction, surpassing other N-containing MOF-derived carbons due to the Lewis-base sites and high porosity. With the assistance of Pd NPs stabilized by N species, the catalyst exhibited superior performance in the tandem Knoevenagel condensation and hydrogenation of substituted benzaldehydes.

Given the high stabilization energy of benzene, the catalytic hydrogenation usually requires harsh conditions and/or supported noble metal (Rh, Ru, or Pt) catalysts [127,128]. For the sake of cost reduction and improvement of the catalytic efficiency, Han and co-workers used MOFs as precursors to synthesize Ni/SiO_2 and Co/SiO_2 with ultrafine particle size of less than 1 nm (Fig. 2b) [118]. The non-noble metal catalysts exhibited superior catalytic activity and stability for the liquid-phase hydrogenation of benzene below 100 °C. The hydrogenation of quinoline is important since the product, 1,2,3,4-tetrahydro quinoline is a major requisite for the synthesis of dyes and medicine [129]. Li, Wu and co-workers reported a precise controllable synthesis of isolated single Ru site stabilized with nitrogen-doped porous carbon (Ru SAs/N–C) by choosing Ru^{3+}@NH_2–UiO-66 as precursor [110]. The atomically isolated dispersion of Ru sites in the matrix was successfully formed with the assistance of the amino groups. The single Ru site coordinated with N behaves as a semi-homogeneous catalyst for the selective hydrogenation of quinolines and their derivatives.

3.1.3. CO_2 fixation reaction

Except for the organic catalytic oxidation and reduction reactions, CO_2 fixation with epoxides has been intensively investigated with the utilization of MOF-derived composites. Toyao et al. successfully prepared bifunctional acid–base catalysts by direct pyrolysis of ZIFs (ZIF-7, -8, -9 and -67) at different temperatures [130]. These materials with Co NPs and N species can separately serve as acid and base sites, exhibiting the highest catalytic activity for the conversion of CO_2 and epoxides into cyclic carbonates under 0.6 MPa of CO_2 at 80 °C. Jiang and co-workers developed an effective approach to synthesizing ZnO NPs encapsulated N-doped porous carbon (ZnO@NPC–Ox) by the pyrolysis of ZIF-8 and subsequent oxidation with sodium hypochlorite [131]. Among all ZnO@NPC–Ox samples, ZnO@NPC–Ox-700 possessed the highest conversion (98%) and selectivity (100%) for the cycloaddition of CO_2 and styrene oxide under mild conditions (60 °C, 0.1 MPa CO_2).

3.2. Gas-phase catalysis

3.2.1. CO oxidation reaction

It is well-known that, the poisonous gas, CO, is produced mostly in metallurgy, graphite electrode manufacturing, or vehicle exhaust every year, which brings about serious environmental pollution and personnel casualties [132]. The conversion and utilization of CO are desired, and meanwhile, the CO conversion has been developed as a well-accepted probe reaction. Previous studies have proved that noble metal active species, such as Au, Pd, or Pt exhibit excellent catalytic performance in CO oxidation [133,134]. Later, different transition metal-based catalysts have also shown their high activity for this reaction. The copper–ceria system has been demonstrated as efficient catalyst for preferential oxidation of CO [135]. Given that the exploration of copper precursors and facile approaches is pivotal to the fabrication of CuO/CeO_2 catalyst, Zhang et al. introduced Ce^{3+} into the channels of Cu–MOF ($Cu_3(BTC)_2$). Then a series of CuO/CeO_2 catalysts with well-dispersed copper species were synthesized by direct pyrolysis of the mixture at different temperatures, which exhibited excellent catalytic activity for preferential CO oxidation in H_2-rich stream [136].

Actually, a number of porous Cu-based nanocomposites, like CeO_2:Cu^{2+} [137], CuO/TiO_2 [138], CuO/Cu_2O [139] with various morphologies and $Cu/CuO_X/C$ [140] derived from Cu–BTC or

Cu–BTC-based composites under different pyrolysis conditions, have been applied for catalytic CO oxidation. These low-cost catalysts showed remarkable activity for CO oxidation under relatively mild conditions. Liu et al. developed well dispersed and size-controllable CuO/TiO_2 porous material featuring superior catalytic performance with the full conversion of CO at 175 °C compared with some supported noble metals [138]. Very recently, another MOF, Cu^{2+}@Ce–UiO-66, was utilized as precursor for the preparation of CuO/CeO_2 catalyst (x-CuCe), which exhibits excellent catalytic performance for preferential oxidation of CO in the H_2-rich stream with the selectivity higher than 99.5% [142]. In addition, Li and co-workers reported Co/C-600 synthesized by pyrolysis of ZIF-67 at 600 °C under argon atmosphere, which performed high catalytic activity for CO oxidation even at −30 °C [143]. The *in situ* Fourier transform infrared spectroscopy (FTIR) experiments conducted under both dry and wet conditions confirmed the tolerability of moisture of the catalyst.

3.2.2. Fischer–Tropsch synthesis

Conversion of syngas ($CO + H_2$) via Fischer–Tropsch (F–T) synthesis has been recognized as one of the most feasible methods for turning syngas into liquid fuels [144]. The F–T synthesis is traditionally catalyzed by Co, Fe and Ru, among which Fe-based catalysts are the most cost-effective for the industrial process [145]. However, many challenges remain unsettled, like the sintering, carbon deposition, agglomeration of iron, phase transition of iron during pyrolysis as well as strong metal-support interactions, which significantly affect the catalytic performance [146]. In order to solve these problems, Santos et al. designed well dispersed Fe NPs embedded in the porous carbon matrix with very high Fe loadings through the pyrolysis of Fe-based MOF Basolite F300 (Fe–BTC) [147]. The obtained Fe@C catalysts with various Fe/C ratios reached very high conversion levels, ranging from 72% to 77% after 90 h on stream. Then a series of catalysts with different pyrolysis temperatures were synthesized by adjusting the loading amount, average particle size and degree of carburization of Fe@C catalysts [148]. *In situ* X-ray absorption fine structure spectroscopy (XAFS), diffuse reflectance infrared Fourier transform spectroscopy (DRIFTS) and Mössbauer spectra were also utilized for explaining the properties of Fe and C during pyrolysis. All of the catalysts retained their stability during 80 h on stream under high temperature conditions (FTY = 0.31–0.38 $mmol_{CO}\ g_{Fe}^{-1}\ s^{-1}$).

An et al. developed new F–T synthesis catalysts, Fe–MIL-88B/C and Fe–MIL-88B–NH_2/C, via simple pyrolysis of Fe–MIL-88B and Fe–MIL-88B-NH_2, respectively (Fig. 3a) [149]. The Fe-time yields (the amount of CO converted to hydrocarbons per gram of Fe per second) of Fe–MIL-88B–NH_2/C were as high as 720 $\mu mol_{CO}\ g_{Fe}^{-1}\ s^{-1}$ under the conditions of 300 °C, 2 MPa and $H_2/CO = 1$, which surpass that of most F–T catalysts reported previously. The authors also discovered that the activity kept rising in the initial 30 h and then stabilized because in the initial stage, the Fe_3O_4 NPs were gradually transformed into χ-Fe_5C_2 on the exterior, which acted as active phase for F–T synthesis. More importantly, the carbonates covering the surface of Fe_3O_4@χ–Fe_5C_2 NPs were resulted from the decarboxylation of MOFs during pyrolysis, which not only helped to protect the NPs but also provided dangling bonds for catalysis. In addition, two typical MOFs, ZIF-67 and Co–MOF-74, were employed as sacrificed templates for the preparation of suitable catalysts for F–T synthesis (Fig. 3b) [150]. The Co–MOF-74-derived Co@C exhibited superior conversion of CO to that of ZIF-67-derived counterparts, which is associated with the larger pore size of the MOF-74-derived carbon, since the diffusion of long-chain hydrocarbons can get enhanced. On the other hand, ZIF-67-derived Co@NC showed a higher selectivity toward short-chain hydrocarbons because the narrower pores and electron donation of N species favor the formation of short-chain products simultaneously.

3.2.3. CO_2 hydrogenation reaction

Conversion of CO_2 to CO via hydrogenation, also known as the reverse water–gas shift (RWGS) reaction, is traditionally catalyzed by noble metal (Pt or Rh) catalysts [152,153]. Among non-noble metal catalysts, Cu is a promising candidate [154]. Unfortunately, Cu has a strong tendency toward aggregation at reaction temperatures above 300 °C [155]. In order to improve Cu-based catalysts, Zhang et al. prepared hierarchical porous Cu@C and Cu/Zn@C

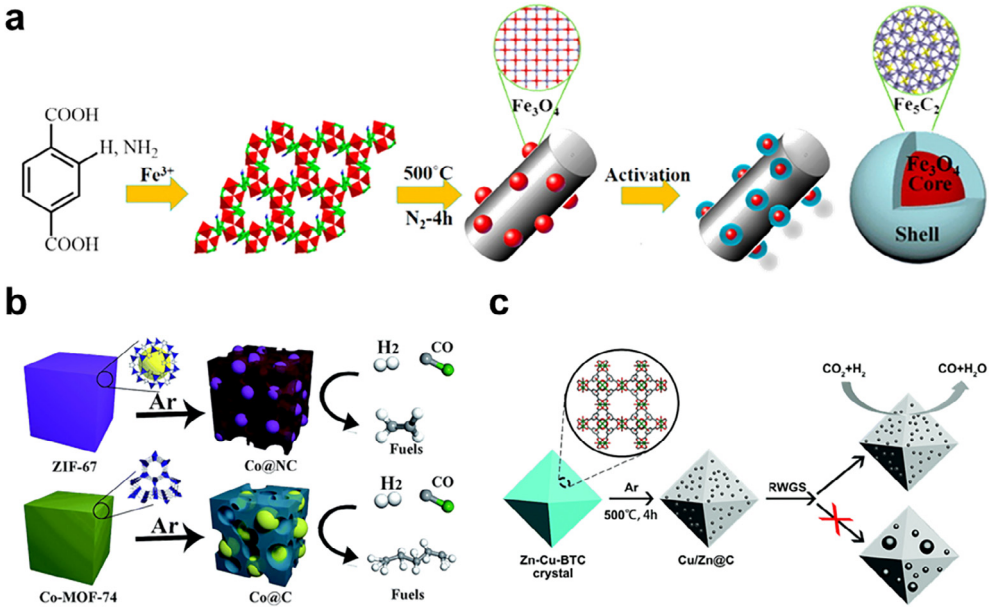

Fig. 3. (a) Schematic illustration presenting the synthesis of Fe–MIL-88B/C and Fe–MIL-88B–NH_2/C nanocomposites from isostructural Fe–MOF precursors. Adapted with the permission from Ref. [149]. Copyright 2016, American Chemical Society. (b) Schematic illustration showing the preparation of MOF-derived F–T catalysts. Reproduced with the permission from Ref. [150]. Copyright 2017, The Royal Society of Chemistry. (c) Preparation of Cu/Zn@C structures for RWGS. Reproduced with the permission from Ref. [156]. Copyright 2017, The Royal Society of Chemistry.

structures via facile pyrolysis of Zn doped Cu-BTC (Fig. 3c) [156]. The Cu/Zn@C catalyst, with synergistic effects between Cu and Zn, exhibited superior activity with 5.0% CO_2 conversion and 100% CO selectivity at 500 °C under a total pressure of 1 bar in comparison with that of Cu@C and previous catalysts.

4. MOF-derived porous materials for photocatalysis

In recent few years, MOF-derived porous composites have been developed as excellent photocatalysts toward various reactions [158–190]. The MOF-derived photocatalysts possess their unique merits. With respect to the compositions, MOFs containing metal nodes can be directly transformed into metal oxides or metal sulfides, some of which are semiconductors. As for their structures, the high porosity of MOF-derived materials facilitates the rapid reaction of charge carriers with the substrates that are accessible to active sites through pores, thus greatly suppressing the recombination of electrons and holes. In this section, we would mostly focus on the latest studies of MOF-derived porous composites on light-driven energy/environment-related reactions including photocatalytic degradation of dyes, water splitting and CO_2 reduction (Table 2).

4.1. Photocatalytic degradation of dyes

MOF-derived porous metal oxides/sulfides, or their porous hybrids are potential photocatalysts for degradation of dyes owing to their low cost, high stability, excellent optical absorption/mass transfer and improved electron-hole separation. The growing research interest in the application of MOF-derived materials for photodegradation of dyes has been reflected by a certain number of publications [160–177]. Photocatalysts with controllable structure, shape and size, such as hybrid composites composed by precious metals and MOF-derived oxides (e.g., Au/ZnO) [162] and MOF-based Co_3O_4/GN [176], C–N-doped ZnO [163] and Fe_2O_3/C [169], have been demonstrated to be excellent photocatalysts for the degradation of dyes in wastewater.

Semiconducting zinc oxide (ZnO), as one of the most promising photocatalytic materials, has been used for degradation of organic pollutants due to its excellent photosensitivity and environmentally friendly behavior [164]. For the sake of the improvement of the catalytic efficiency and enhancement of long-term and cyclic stability of ZnO catalyst, several novel ZnO-based porous materials have been fabricated from ZIF-8 and shown better catalytic efficiency in decomposition of dyes compared with traditional TiO_2 due to their unique morphology, high surface area and ordered porosity. For instance, Cao et al. synthesized 3D graphene network (3DGN) for the growth of ZIF-8 polyhedrons [165]. Upon annealing under argon atmosphere, 3DGN loaded with ZnO NPs was obtained. Under UV irradiation for 60 min, methylene blue was totally decomposed, exceeding the performance of pure 3DGN or ZnO, which can be ascribed to the high surface area of the composite and effective interaction between the metal oxides and the graphene framework. Recently, Chen et al. presented the fabrication of a metal oxide@carbon core–shell hybrid by direct pyrolysis of a hollow ZIF-67@ZIF-8 matrix under an inert atmosphere (Fig. 4) [166]. The obtained ZnO@C–N–Co was constructed with uniform ZnO particles as core and N-doped graphitized carbon embedded with Co NPs as the shell layer. It is noteworthy that the suitable pyrolysis temperature was very important for the successful preparation of ZnO@C–N–Co during pyrolysis as the inappropriate temperature is unfavorable to the formation of ZnO core. Encouraged by the abundant mesopores and unique structural advantages, the photodegradation performance of ZnO@C–N–Co was further examined. As expected, the as-synthesized ZnO@C–N–Co exhibited higher degradation percentage (99.5%) and excellent magnetic recyclability in the photocatalytic degradation of methyl orange (MO), than those of pure ZnO (60.2%), ZIF-8-600 (41.9%) and ZIF-67-600 (29.4%) after 2.5 h of light irradiation. The superior catalytic performance of ZnO@C–N–Co was mainly ascribed to

Table 2
Summary of MOF-derived porous materials for photocatalytic reactions.

Catalyst	MOF precursor	Catalytic reaction	Refs.
MgO	Mg–MOF	Photodegradation	[161]
Au/ZnO	ZIF-8	Photodegradation	[162]
C–N-doped ZnO	ZIF-8	Photodegradation	[163]
3DGN	ZIF-8	Photodegradation	[165]
ZnO@C–N–Co	ZIF-67@ ZIF-8	Photodegradation	[166]
RGO@ZnO	ZIF-8	Photodegradation	[167]
ZnO	ZIF-8	Photodegradation	[168]
Fe_2O_3/C	MIL-88A(Fe)	Photodegradation	[169]
γ-Fe_2O_3/C	MIL-53(Fe)	Photodegradation	[170]
In_2O_3/Co_3O_4	In/Co–MOFs	Photodegradation	[171]
TiO_x/C	ZTOF-1	Photodegradation	[172]
SOS@ZnO	ZIF-8	Photodegradation	[173]
TiO_x/C	MIL-125	Photodegradation	[174]
ZnO	MOF-5	Photodegradation	[175]
Co_3O_4/GN	ZIF-67	Photodegradation	[176]
Fe_3O_4@C/Cu	Fe_3O_4@ HKUST-1	Photodegradation	[177]
Fe_2O_3/TiO_2	Fe–MIL-101	Hydrogen production	[178]
Cu/Cu@TiO_2	MIL-125(Ti)	Hydrogen production	[179]
CdS	Cd–Fe–PBA	Hydrogen production	[180]
$Zn_{0.30}Co_{2.70}S_4$	ZnCo–MOFs	Hydrogen production	[181]
ZNGs	ZIF-8	Hydrogen production	[182]
Co_3O_4/TiO_2	Co–MOF	Hydrogen production	[183]
CdS	MIL-53	Hydrogen production	[184]
Pt–ZnO–Co_3O_4, Pt–ZnS–CoS, Pt–Zn_3P_2–CoP	ZnCo–ZIF	Hydrogen production	[185]
T–CoO_x–C	ZIF-67	Water oxidation	[186]
Co_3O_4	POM@MOF	Water oxidation	[187]
Fe@C	Fe–MIL-101	CO_2 reduction	[189]
In_2S_3–$CdIn_2S_4$	MIL-68	CO_2 reduction	[190]

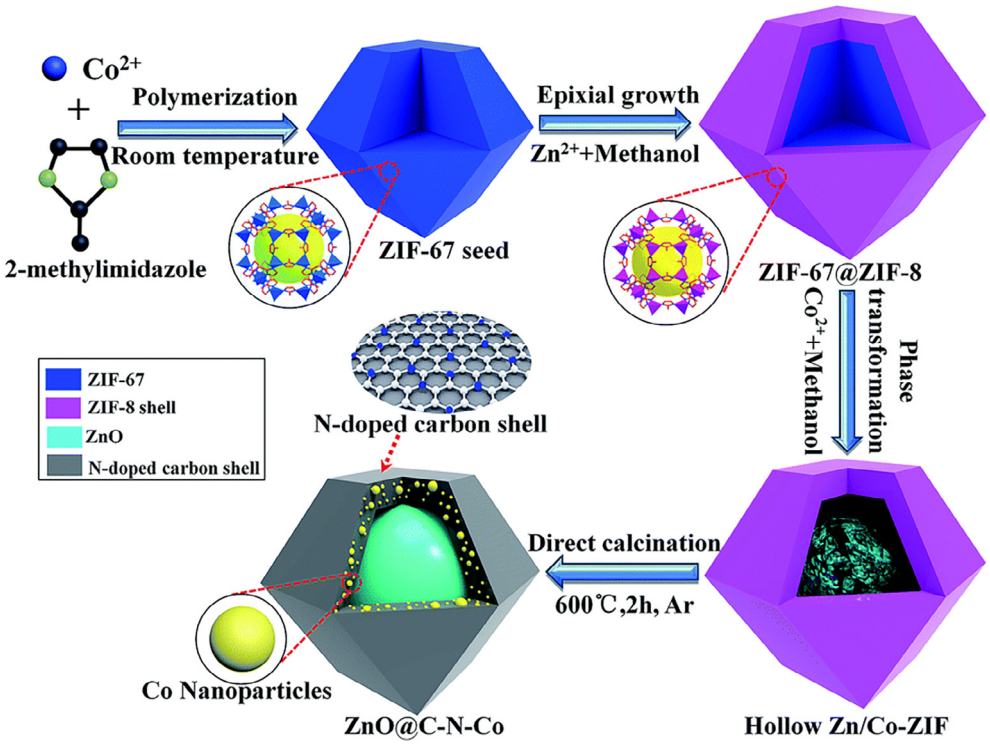

Fig. 4. Schematic illustration of the preparation of core–shell ZnO@C–N–Co catalyst. Reproduced with the permission from Ref. [166]. Copyright 2017, The Royal Society of Chemistry.

the porous structure, high surface area and synergistic effects between the C–N–Co shell and the ZnO core.

Given that most of as-prepared porous metal oxides usually catalyze the photocatalytic reaction under ultraviolet light irradiation due to their large bandgap, it is desired to develop effective photocatalysts responsive to visible light. Recently, Zhu et al. have successfully prepared reduced graphene oxide (RGO) incorporated MOF-derived ZnO composite via the microwave assisted method and it has been applied for catalytic degradation of methylene blue (MB) [167]. The obtained composite with 1.5 wt% RGO showed an optimal photocatalytic activity and stability compared with those of pure ZnO and other composites with different contents of RGO, due to the increased visible light absorption and the interaction between ZnO and RGO. Pan et al. prepared ZnO–carbon composites through the pyrolysis of ZIF-8 [168]. Results show that the performance of photocatalytic degradation of organic dyes is positively associated with the carbon content, as the carbon dopant effectively prohibits the recombination of photo-induced electrons and holes. Besides, carbon dopant can reduce the gap between conduction band and the Fermi level, realizing the absorption of visible light.

In addition, other novel MOF-derived porous metal oxides, such as Fe_2O_3/C [169], [170] and In_2O_3/Co_3O_4 [171], have been demonstrated to be excellent photocatalysts for the degradation of dyes. Xu et al. synthesized In_2O_3/Co_3O_4@palygorskite via the pyrolysis of Co/In–MOF@palygorskite at 500 °C in air for 2 h [171]. The obtained catalyst showed excellent activity toward the degradation of organic dyes, which can be assigned to the participation of palygorskite. The palygorskite not only provides large pore volumes for the adsorption of dye molecules, but also reinforces the separation of photo-induced electrons and holes.

4.2. Photocatalytic H_2 production

It has been well demonstrated that, the activity of photocatalytic water splitting is strongly related to the photo-absorption capability, bandgap energy, the types of active sites/co-catalysts and charge separation/transfer properties, etc. In recent years, various methods have been intensively explored aiming to increase the charge separation/transfer efficiency and improve the catalytic performance. Traditionally, as a well-known photocatalyst, TiO_2 has been used for various photochemical reactions. However, with the large bandgap, TiO_2 only has the absorption of UV light, which occupies about 5% of sunlight. To adequately utilize abundant solar energy source and reduce cost, great efforts have been dedicated to developing photocatalysts which can absorb visible light and effectively catalyze water reduction/oxidation.

Although TiO_2 can effectively catalyze water reduction, it only absorbs UV light. Meanwhile, Fe_2O_3 is able to absorb visible light, while its conduction band is too low to drive H_2 generation. To solve these issues, Lin and co-workers have attempted to use nanoscale MOFs as sacrificial templates for the synthesis of Ti based core–shell structure nanocomposites by pyrolysis of Fe–MIL-101 coated with TiO_2 under air atmosphere, which were then utilized as support for Pt NPs [178]. Interestingly, the thickness of the coated TiO_2 could be adjusted by controlling the concentration of acid or the reaction time. The resulted Fe_2O_3@TiO_2/Pt with the retaining of porosity and octahedral structure showed linear increase of the H_2 amount produced during the entire period of photocatalytic water reduction, realizing a total of 30.0 μmol H_2 per mg of material produced after 48 h under visible light. The better activity of Fe_2O_3@TiO_2/Pt than those of Fe_2O_3 or TiO_2 alone or their physical mixture mainly takes advantage of the synergy between Fe_2O_3 and TiO_2.

Not limited to metal oxides, MOF-derived metal sulfides can also be utilized as co-catalysts for photocatalysis. Su et al. synthesized yolk-shell CdS microcubes via the sulfidation of Cd–Fe PBA under microwave-assisted hydrothermal conditions [180]. At the beginning of the sulfidation, ion exchange between S^{2-} and Fe complex ion took place on the exterior of MOFs. Then the sulfidation proceeded on the outer layers, which contributed to

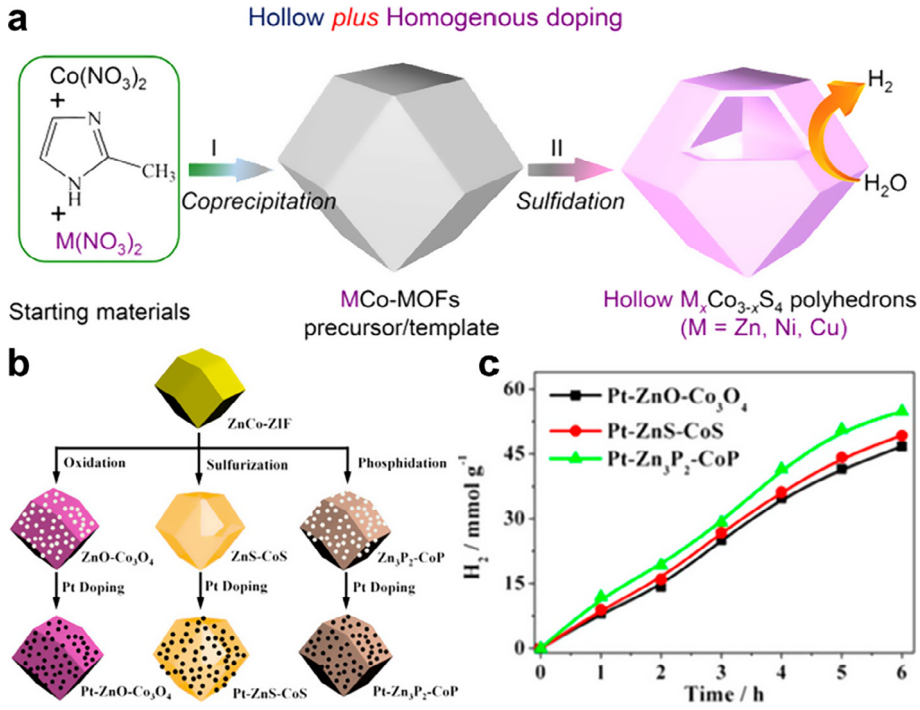

Fig. 5. (a) Schematic illustration of the preparation of hollow $M_xCo_{3-x}S_4$ for photocatalytic hydrogen production. Reproduced with the permission from Ref. [181]. Copyright 2016, American Chemical Society. (b) Schematic illustration of the fabrication of Pt–ZnO–Co_3O_4, Pt–ZnS–CoS and Pt–Zn_3P_2–CoP photocatalysts. (c) The comparison of photocatalytic performance of Pt–ZnO–Co_3O_4, Pt–ZnS–CoS and Pt–Zn_3P_2–CoP. Adapted with permission from Ref. [185]. Copyright 2017, Elsevier.

the separation of MOF core and CdS layer. Finally, the unique structure was obtained, exhibiting excellent photocatalytic H_2 production with a H_2 evolution rate of 3051.4 μmol h^{-1} g^{-1}. Similarly, Huang et al. selected bimetallic MOF (MCo–MOFs, M = Ni, Cu, Zn) as the precursor for the fabrication of bimetallic sulfides (Fig. 5a) [181]. After subsequent sulfidation, the hollow polyhedra were generated. The system ($Zn_{0.30}Co_{2.70}S_4$) exhibited good photocatalytic performance toward hydrogen production, with a rate of 1 55.2 μmol h^{-1}, which can be ascribed to the homogeneous distribution of metal elements and the hollow structures.

Jiang and co-workers have chosen thermally stable MOF, MIL-53(Al), as hard porous templates for metal sulfide construction. Several metal nitrates as precursors were initially incorporated into the pores of MOFs for the formation of metal oxide replica, which were subsequently converted to metal sulfides within MOFs during nanocasting process [184]. The hierarchically porous CdS was finally obtained after MOF removal and exhibited excellent performance in photocatalytic water splitting for H_2 generation with a rate of 634.0 μmol g^{-1} h^{-1}, far exceeding that of the bulk and nanosized CdS counterparts, which can be attributed to the nanosize effect and the pore structure.

It is noteworthy that the construction of heterojunctions can bring about the enhancement of the photocatalytic activity. In view of this, Li and co-workers used bimetallic MOF as template for the fabrication of heterojunction photocatalysts via the facile oxidation, sulfurization and phosphorization treatment of bimetallic MOF (ZnCo–ZIF) and following doping of Pt NPs (Fig. 5b) [185]. The obtained Pt–ZnO–Co_3O_4, Pt–ZnS–CoS and Pt–Zn_3P_2–CoP exhibited superior photocatalytic activity with the hydrogen generation rate reaching ~7.80, ~8.21 and ~9.15 mmol h^{-1} g^{-1}, respectively, which were higher than those of pure ZIF-8 or ZIF-67-derived porous materials (Fig. 5c). The excellent catalytic performance of the resultant composites was ascribed to their porous structures, large surface areas, synergetic effects between the heterojunction and noble metal, which effectively facilitated the electron-hole separation and fast electron transfer.

4.3. Photocatalytic water oxidation

The porous composites obtained from MOF precursors can also be directly utilized for photocatalytic water oxidation. For instance, Lu and co-workers developed an efficient and economical water oxidation catalyst, named *T*–CoO_x–C, via pyrolysis of ZIF-67 [186]. The optimal 700–CoO_x–C exhibited excellent photocatalytic activity for water oxidation with high TOF of 0.039 ± 0.03 s^{-1} by using $Ru(bpy)_3(PF_6)_3$ as an oxidant, which can be assigned to the large surface area, nitrogen doping and uniform distribution of CoO_x species. Later, Lan et al. successfully prepared molecular cluster@oxide catalyst through the introduction of polyoxometalates (POMs) as guests into the pores of ZIF-67, followed by pyrolysis in air [187]. The resultant POM@Co_3O_4 exhibited significantly improved photocatalytic O_2 production compared with the corresponding pure MOF-derived nanocomposite, since the electrons from the conduction band of Co_3O_4 could be transferred to the POM under visible light irradiation, greatly improving the separation of holes and electrons.

4.4. Photocatalytic CO_2 conversion

The efficient capture and catalytic transformation of CO_2 into fuels such as CH_4 or CO are deemed to be an effective approach addressing the energy crisis [188]. Recently, Ye's group have successfully constructed an elegant porous nanocomposite (Fe@C) with iron NPs as core and ultrathin (1–3 layers) carbon layers as shell via simple pyrolysis of Fe–MIL-101 template (Fig. 6a) [189]. Due to the photothermal effect, the local temperature of NPs rises under light irradiation, which provides adequate energy for the reaction. Besides, the local surface-plasmon resonances of Fe can be utilized for the activation of CO_2. Furthermore, the confinement of the carbon layer would contribute to the selectivity to CO. Thanks to these advantages, the core–shell Fe@C catalyst produced 2196.17 μmol CO after photoirradiation for 120 min, exceeding the

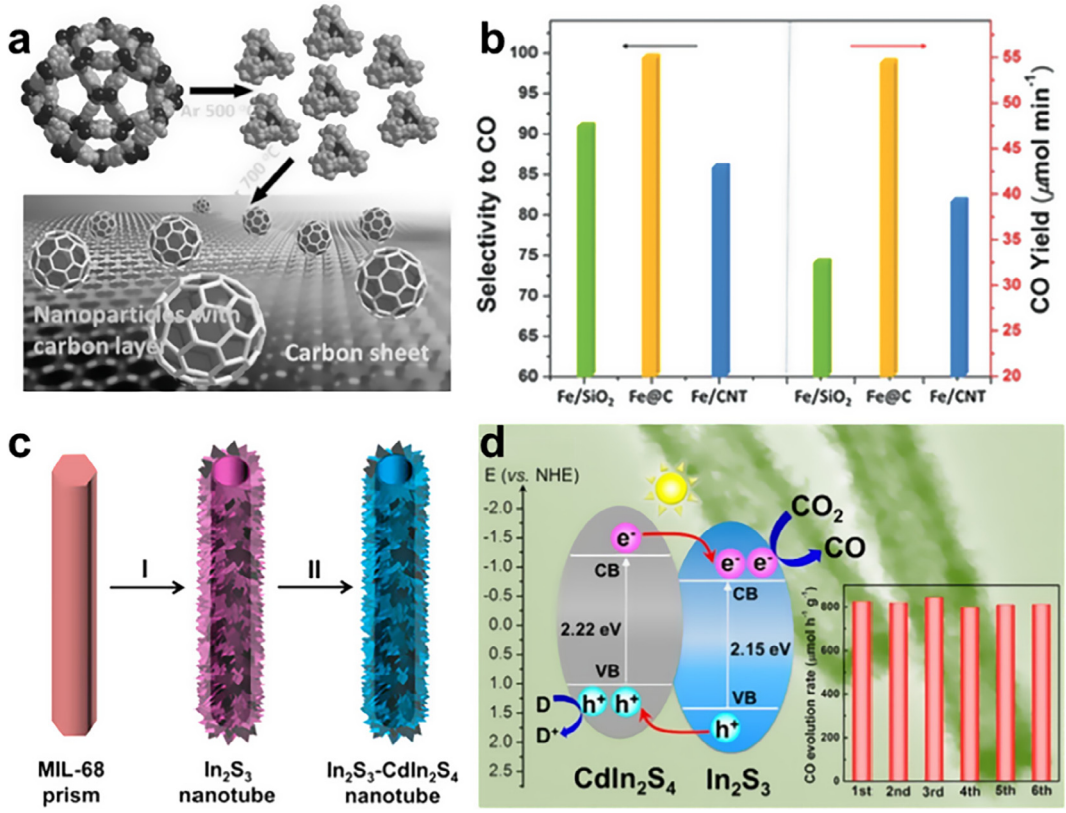

Fig. 6. (a) Schematic illustration showing the fabrication of the core–shell structured Fe@C hybrid. (b) CO selectivity and yield of different catalysts toward photocatalytic CO_2 reduction. Adapted with the permission from Ref. [189]. Copyright 2016, Wiley-VCH. (c) Schematic illustration of the synthesis of In_2S_3–$CdIn_2S_4$ heterostructured nanotube and (d) its band structure and recyclability for photocatalytic CO_2 reduction. Adapted with the permission from Ref. [190]. Copyright 2017, American Chemical Society.

CO_2 conversion over Fe/SiO_2 and Fe/CNT catalysts under the same reaction conditions (Fig. 6b).

In view of the sluggish separation kinetics of the electrons and holes in metal sulfides, Wang et al. prepared In_2S_3–$CdIn_2S_4$ heterostructured hierarchical nanotubes for photocatalytic reduction of CO_2 (Fig. 6c and d) [190]. By utilizing solution infiltration method followed by heat treatment, MIL-68 prisms were initially transformed into In_2S_3 nanotubes, which subsequently underwent cation exchange for the fabrication of heterostructured nanotubes. The nanotubes exhibited superior selectivity toward the photocatalytic conversion of CO_2 under visible light irradiation, with a high rate of 825 μmol h^{-1} g^{-1}, far exceeding that of In_2S_3 photocatalyst, which is associated with the unique heterostructure (beneficial for the mobility and separation of electrons and holes) and large surface area (promoting the adsorption of CO_2).

5. MOF-derived porous materials for electrocatalysis

With the rapid consumption of traditional fossil fuels, the development of earth-abundant and renewable energy resources has thus become a hot research topic. Electrochemical energy-related applications, including ORR, oxygen evolution reaction (OER), hydrogen evolution reduction (HER), methanol oxidation reaction (MOR), CO_2 reduction reaction (CO_2RR), etc., have been intensively investigated in recent years. To date, the state-of-the-art catalysts mainly depend on noble metals (e.g., Pt, Pd and Ru). Nevertheless, stability and high cost of noble metals impede their large-scale application in industry. In view of those drawbacks, transition metal (Fe, Co, Ni, Zn, etc.)-based MOFs have been widely used for the preparation of porous carbons, metal-based compounds and their hybrids for improved electrocatalytic performance [191–202,207–235]. The main advantages of MOF-based electrocatalysts can be summarized as follows. Firstly, the pyrolysis of MOFs gives carbon-based catalysts, which greatly enhance the conductivity in reference to original MOFs, facilitating electron transfer during electrocatalysis. In addition, the inherited large surface area and high porosity in the resultant composites are beneficial to the access and dispersion of high-density active sites. Finally, compared with the MOF precursors, the stability of derived porous materials can be greatly enhanced, bringing about excellent recyclability. Given the above-mentioned factors, MOF-derived porous materials are promising candidates for various electrocatalytic processes (Table 3).

5.1. Oxygen reduction reaction

The ORR is one of the most important cathodic reactions in many energy conversion technologies, such as fuel cells and metal–air batteries, where Pt-based catalysts are always employed to accelerate the sluggish kinetics. To reduce the high cost of noble metals, MOF-derived materials have attained explosive development and provided a good alternative for Pt-based ORR electrocatalysts in the past few years [193–202,207–216]. As a seminal work in MOF-derived materials for ORR, a cobalt imidazolate framework was selected as the precursor for the synthesis of electrocatalysts with high-density and regularly distributed Co–N_4 centers [195]. After the pyrolysis at 750 °C under argon atmosphere for 1 h followed by acid leaching to remove metallic Co NPs, the catalysts featured Co–N_4 active sites, with an onset potential of 0.83 V *vs* RHE. Given that the Fe-containing catalysts sometimes tend to be

Table 3
Summary of some MOF-derived porous materials for corresponding electrocatalytic reactions.

Catalyst	MOF precursor	Catalytic reaction	Refs.
Pt–Ni/PC 950	MOF-5	ORR	[193]
Co–N_4	Cobalt imidazolate framework	ORR	[195]
FeIm/ZIF-8	Iron imidazolate framework	ORR	[196]
Carbon-L	ZIF-7	ORR	[197]
NCNTFs	ZIF-67	ORR	[198]
N-CNTs-650	ZIF-67	ORR	[199]
Z8-Te-1000	ZIF-8	ORR	[200]
ZIF-S-p	ZIF-67	ORR	[211]
Co@Co_3O_4@C-CM	ZIF-9	ORR	[212]
NC900	ZIF-8	ORR	[84]
GNPCSs-800	ZIF-8	ORR	[90]
NCNTs-20	Zn–Fe–ZIF	ORR	[202]
Fe–N–C	Fe/Phen/ZIF-8	ORR	[207]
Co SAs/N–C	Zn/Co–ZIF	ORR	[208]
Fe–ZIF	Fe-doped ZIF-8	ORR	[209]
CNPs	MIL-88B–NH_2	ORR	[213]
CPM-99Fe/C	CPM-99	ORR	[215]
$FeCo_2$–NPC-900	PCN-224–FeCo	ORR	[216]
CoP@BCN	Co–MOF	HER	[220]
NiS	Ni–Co PBA	HER	[95]
MoC_x	POMs@MOFs	HER	[85]
WC	$W(CO)_6$@MAF-6	HER	[79]
MoO_2@PC–RGO	Cu-based POMOFs/GO	HER	[221]
A–Ni–C	Ni–MOF	HER	[222]
$CoFe_2O_4$/C NRAs	MOF-74–Co/Fe	OER	[227]
NiCoP/C	ZIF-67@LDH	OER	[223]
Fe–Ni–P/rGO-400	PCN-600–Ni	OER	[224]
NGO/Ni_7S_6	Ni–MOF	OER/HER	[225]
Co_3S_4@MoS_2	ZIF-67	OER/HER	[226]
CoP/rGO-400	ZIF-67/GO	OER/HER	[92]
Ni@CoO@CoNC	Ni@CoO@ZIF-67	OER/HER	[94]
CoS_2 NTA/CC	Co–MOF	OER/HER	[231]
Co_3O_4–C	Co–MOF	ORR/OER	[93]
NC@Co–NGC	ZIF-8@ZIF-67	ORR/OER	[230]
Pd/ZC-1000	ZIF-8	MOR	[232]
Ni SAs/N–C	$Ni(NO_3)_2$@ZIF-8	CO_2RR	[233]
C–AFC@ZIF-8	AFC@ZIF-8	CO_2RR	[83]
Pd/Co–N/carbon	Co–ZIF/graphene oxide (GO)	Dimethylation	[234]

more active than Co-containing catalysts, the Fe-containing electrocatalyst was synthesized through the ball-milling of the mixture of Fe–MOF and ZIF-8, the pyrolysis under argon atmosphere for 1 h at 1050 °C and subsequent annealing under NH_3 atmosphere at 950 °C for 15 min [196]. The catalyst exhibited excellent ORR performance, with an onset potential of 0.915 V *vs* RHE and four-electron process, which can be assigned to the large surface area and high N content of the catalyst. Similarly, by using ZIF-7 as a precursor and environment-friendly glucose as an additional carbon source, Cao and co-workers prepared two kinds of ZIF-derived N-doped porous carbons (marked as Carbon-L and Carbon-S) [197]. When performed as ORR catalyst, the Carbon-L exhibited superior ORR performance to commercial 20% Pt/C catalyst.

Carbon nanotubes (CNTs), with unique physical and chemical properties, have attracted great interest for many potential applications. However, the tedious preparation of CNTs restricts their applications. Recently, Xia et al. have successfully fabricated N-doped CNTs (NCNTs) by simple pyrolysis of ZIF-67 in H_2/Ar atmosphere at high temperatures (>600 °C) [198]. The CNTs were catalytically growing by the generated Co NPs in the presence of H_2. Thanks to their unique features in hollow structure, optimum graphitic degree and N doping, the resultant NCNTs exhibited enhanced activity, durability and methanol tolerance for ORR. By contrast, Meng et al. also developed another facile and general approach for the oriented formation of CNTs from ZIFs (Co, Fe–ZIF, ZIF-67, Ni–ZIF) via a low-temperature pyrolysis under argon atmosphere for a long period of time [199]. The optimal N–CNTs-650 catalyst showed excellent ORR activity with half-wave potential of 0.85 V *vs* RHE, surpassing that of other N–CNTs–T counterparts investigated and Pt/C.

As another well-known Zn-based MOF sharing the same topology with ZIF-67, ZIF-8 is a promising candidate for the preparation of N-doped porous materials. In 2014, Xu and co-workers have successfully synthesized N-decorated nanoporous carbons with high surface area by using ZIF-8 as a template and furfuryl alcohol as the secondary carbon along with NH_4OH as the additional nitrogen sources (Fig. 7a) [84]. The N-decorated NC900 showed an ORR onset potential at 0.83 V *vs* RHE, attributed to the high surface area, proper channels and abundant nitrogen sites. Given the limited degree of graphitization of the resultant porous carbons via ZIF-8 pyrolysis, Zhang and co-workers successfully increased the electrical conductivity by *in situ* anchoring of ZIF-8 on GO and carbonization to GNPCSs at different temperatures [90]. Thanks to the synergistic effect between NC and graphene, high surface area, well-defined porous structures and abundant N content, the optimized GNPCSs-800 exhibits a half-wave potential of 0.82 V *vs* RHE and excellent durability, which are superior to commercial Pt/C catalyst. Furthermore, Zhang et al. successfully synthesized highly porous doped carbon nanofibers by pyrolysis of uniform ZIF-8 nanofibers obtained via ultrathin tellurium nanowires (TeNWs) as templates (Fig. 7b) [200]. The optimized Z8–Te-1000 shows half-wave potential of ~−0.226 V *vs* Ag/AgCl for ORR in O_2-saturated 0.1 M KOH. After subsequent P doping, the P–Z8-1000 exhibits a half-wave potential of ~−0.161 V *vs* Ag/AgCl, which is better than the commercial Pt/C catalyst.

The incorporation of catalytically active elements (e.g., Fe) into ZIF-8 has been applied for the fabrication of high performance electrocatalysts. Proietti et al. synthesized Fe-based ORR electrocatalyst derived from ZIF-8 [201]. In their experiment, iron(II) acetate and 1,10-phenanthroline served as Fe and N sources respectively. Then the mixture of the above precursors and ZIF-8 underwent ball-milling and pyrolysis. By altering the parameters including the atmosphere, pyrolysis time and the mass ratio of phenanthroline to the ZIF-8 host, the optimized catalyst possessed an activity of 1120 A g^{-1} at 0.8 V. Li, Yang and co-workers fabricated the N-doped carbon nanotubes (NCNTs) through the pyrolysis of Zn–Fe–ZIF under N_2 atmosphere at 900 °C for 4 h and subsequent acid leaching (Fig. 7c) [202]. The introduction of dicyandiamide induces the formation of NCNTs at low temperature and provides extra nitrogen for NCNTs (denoted as NCNTs–x), resulting in the improved ORR activity. The Fe and Fe_3C formed during pyrolysis further catalyze the formation of NCNT structure at high temperature.

Single atom catalysts (SACs), emerging as a significant research frontier, have attracted intensive attention due to their unique advantages [203–205]. However, many challenges in the preparation and characterization of single atoms remain unsettled. Beyond the synthesis of ultrafine nanoparticles and their composites, MOFs also show precise control on metal sites at atomic level, due to their intrinsic structural features, making them potential candidates for the preparation of SACs [206–209]. More specifically, the high porosity of MOFs and their composites is very helpful for the fabrication of atomically active sites and effectively improves the stability of SACs. In addition, the metal–oxo clusters of MOFs can act as anchoring sites to bind metal ions. Furthermore, some organic linkers of MOFs may offer additional coordination sites to connect single atoms. For example, Jiang and coworkers prepared single Pt atom catalyst by taking advantage of a porphyrinic MOF, Al–TCPP, for photocatalytic H_2 production [206]. The single Pt atoms are located in the porphyrin centers of the ligand, exhibiting superior photocatalytic activity for H_2 production to that of Pt NPs, with a TOF of 35 h^{-1}. This is the first time that

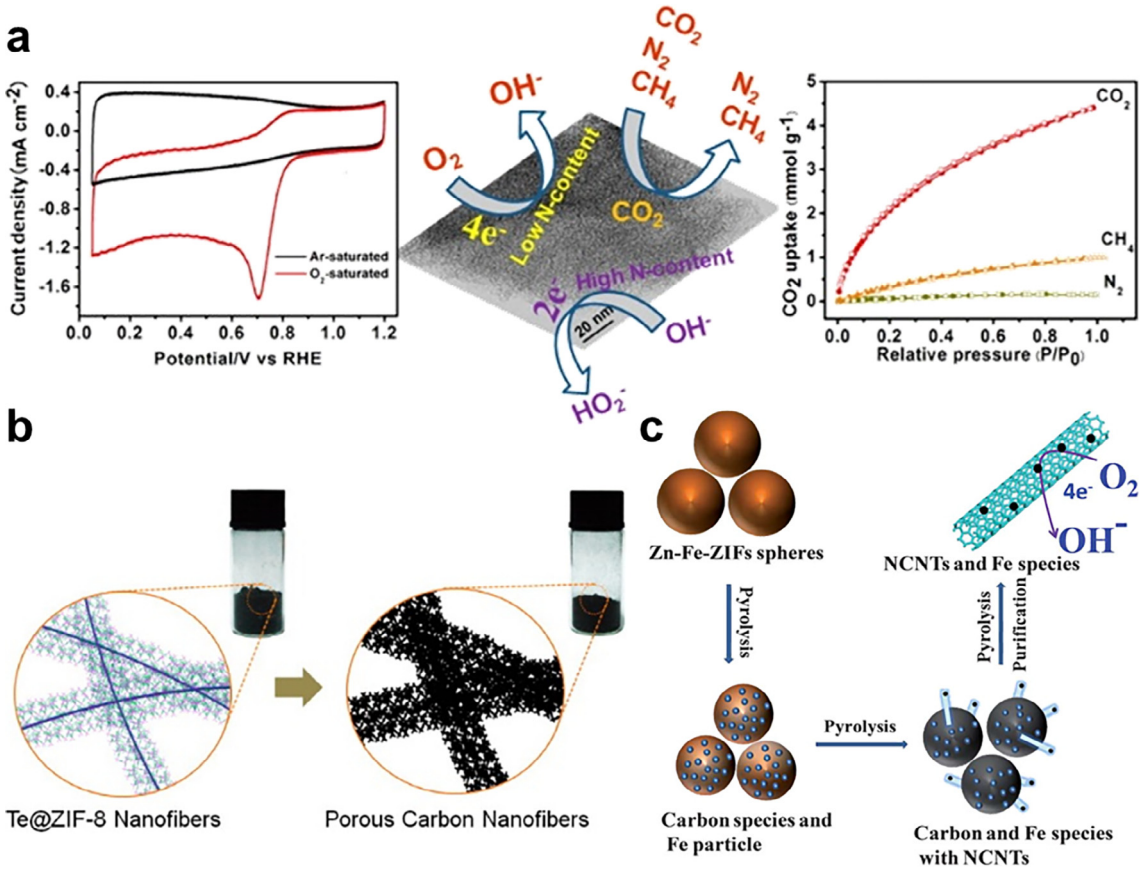

Fig. 7. (a) Schematic illustration of N-decorated nanoporous carbons derived from the FA–NH_4OH/ZIF-8 composites as well as their application in electrocatalytic ORR and CO_2 uptake. Adapted with the permission from Ref. [84]. Copyright 2014, American Chemical Society. (b) The synthesis of porous carbon nanofibers via the pyrolysis of Te@ZIF-8 nanofibers. Adapted with the permission from Ref. [200]. Copyright 2014, American Chemical Society. (c) Synthetic procedures of the N-doped carbon nanotubes. Reproduced with the permission from Ref. [202]. Copyright 2013, The Royal Society of Chemistry.

MOFs directly serve as supports for the stabilization of single atoms with preserved structural integrity. Not limited to pristine MOFs, MOF-derived porous materials can also act as hosts for the synthesis of single atom catalysts. Using iron-acetate/phenanthroline/ZIF-8 (Fe/Phen/ZIF-8) as precursor, Zitolo et al. obtained Fe–N–C catalysts and then investigated their structures of the active sites for ORR [207]. XAFS demonstrated the formation of Fe-centered moieties (FeN_4C_{12}) in the Fe–N–C catalyst, which effectively catalyzed the four-electron reduction of oxygen to water based on the highly basic N-groups formed during the pyrolysis in NH_3 atmosphere. Yin et al. successfully synthesized Co single atoms/nitrogen-doped porous carbon (Co SAs/N–C) from Zn/Co–ZIF [208]. The addition of Zn affects the distance of adjacent Co atoms and provides more free N sites after pyrolysis, inhibiting the aggregation of Co atoms effectively. Co SAs/N–C revealed good ORR activity with a half-wave potential of 0.881 V *vs* RHE and excellent stability, superior to that of commercial Pt/C and most of previous non-precious metal catalysts. Wu, Shao and co-workers developed a chemical doping approach to the synthesis of single-atom Fe catalyst by choosing Fe-doped ZIF-8 as a precursor [209]. The catalyst exhibited remarkable ORR performance in 0.5 M H_2SO_4. These findings would open up an important approach to the synthesis of single-atom metal catalysts based on MOF precursors.

Though the porous carbons derived from ZIF-67 possess certain degree of graphitization as well as Co–N active sites dispersed in the carbon matrix, the limited surface area will restrict the mass transfer, which is closely related to ORR activity. By contrast, the derivation of ZIF-8, which shares the same topology with ZIF-67, can provide large surface area for the carbon matrix, while the obtained products lack graphitization and Co–N active sites. With these in mind, Chen et al. have creatively designed and synthesized the bimetallic MOFs (BMZIFs) based on isomorphism of ZIF-67 and ZIF-8, for the first time (Fig. 8a) [210]. The unprecedented BMZIF-derived porous carbons inherited respective advantages of carbons from ZIF-8 (large surface area) and ZIF-67 (high degree of graphitization and uniform distribution of N and CoN_x active species), thus exhibiting excellent ORR activity comparable to commercial Pt/C under alkaline condition. Especially, upon doping with additional phosphorus, the P–CNCo-20 presented dramatically more positive half-wave potential (−0.12 V *vs* Ag/AgCl) in electrocatalytic ORR, outperforming most of previous MOF derivatives and commercial Pt/C.

In order to optimize the mass transport during electrocatalytic ORR, Guo, Zou and co-workers synthesized Co@Co_3O_4@C NPs embedded in the matrix of porous carbon (Fig. 8b) [212]. The carboxyl groups on the exterior of the carbon matrix (CM) were used for the anchoring of Co^{2+}, which were further utilized for MOF growth. Then the Co-based MOFs were transformed into Co@Co_3O_4 NPs via pyrolysis under argon atmosphere and subsequent oxidation. The ORR performance of Co@Co_3O_4@C–CM is comparable to Pt/C and exceeds that of Co@Co_3O_4@C without carbon matrix. This work reveals a crucial role of the introduction of a highly ordered carbon matrix into the MOF-derived material in improving the ORR activity and stability.

Apart from above extensively investigated ZIFs as precursors, some Fe-based MOFs, such as MIL-88(Fe), MIL-101(Fe) and Fe–porphyrinic MOFs, have also been used as excellent precursors to

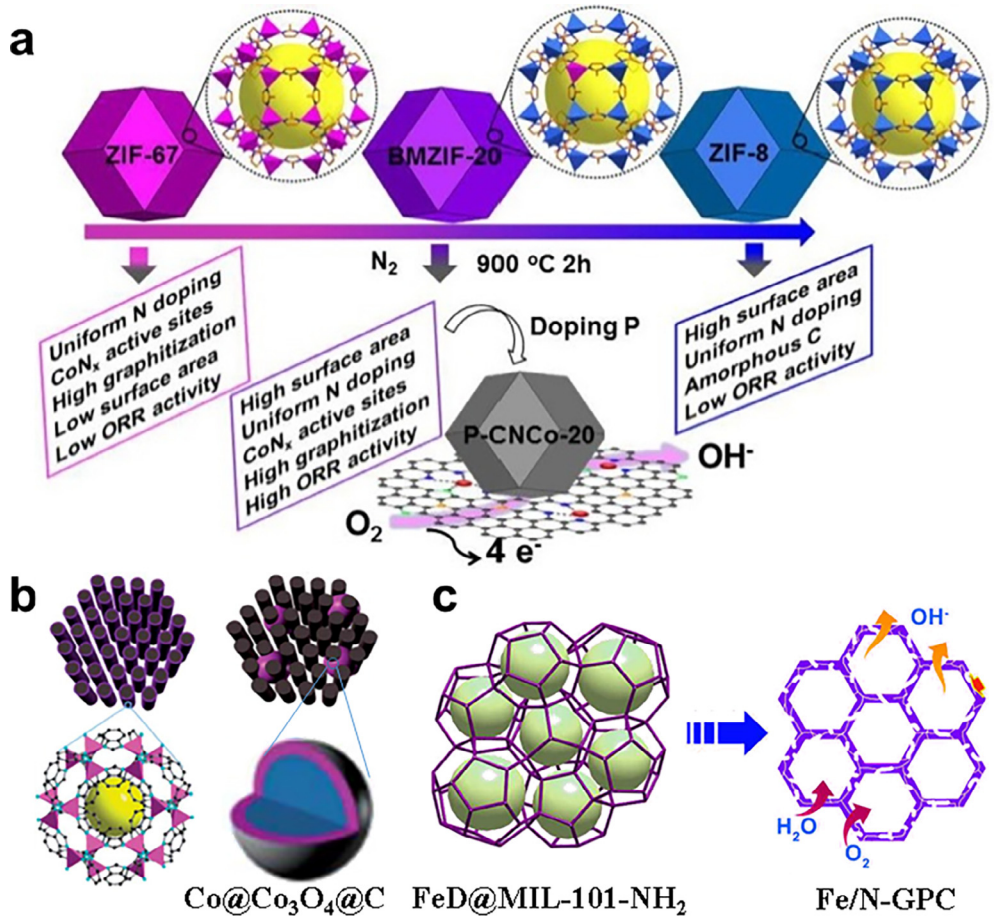

Fig. 8. (a) Illustration of the preparation and respective merits of porous carbon materials from BMZIFs, pure ZIF-67 and ZIF-8 for highly efficient oxygen reduction reaction. Reproduced with the permission from Ref. [210]. Copyright 2015, Wiley-VCH. (b) Schematic illustration of the structure of $Co@Co_3O_4@C$–CM electrocatalysts. Adapted with the permission from Ref. [212]. Copyright 2015, The Royal Society of Chemistry. (c) Pyrolyzed fabrication of the Fe/N–GPC electrocatalysts for ORR. Adapted with the permission from Ref. [88]. Copyright 2017, American Chemical Society.

synthesize highly active ORR electrocatalysts. Zhu et al. obtained atomically dispersed Fe active sites embedded in the hierarchical porous carbon matrix through the introduction of guest species ($FeCl_3$ and dicyandiamide) into the pores of MIL-101–NH_2 and subsequent pyrolysis (Fig. 8c) [88]. Owing to the synergy between the atomically distributed active sites and the hierarchically porous structure, Fe/N–GPC showed excellent activity under alkaline conditions. In addition, Zhao et al. prepared carbonized nanoparticles (CNPs-T) with ultrahigh surface area and ordered porous structure through the facile carbonization of MIL-88B–NH_2 at various temperatures [213]. The optimized catalyst possesses a high catalytic activity toward ORR, with the half-wave potential of 0.92 V *vs* RHE in 0.1 M KOH, surpassing most of the reported non-noble metal catalysts. Considering that the relatively low ratio between metal and carbon is beneficial to improve the performance of ORR catalysts, Qian et al. synthesized N-doped porous carbon materials containing Fe and Fe_3C through the pyrolysis of MIL-88c–Fe and dicyandiamide mixture under argon atmosphere for 2 h [214]. The optimized catalyst (denoted as Fe/NC800) exhibited electrocatalytic activity and methanol tolerance preferable to Pt/C.

Lin et al. employed cubic zirconium–porphyrin frameworks, CPM-99 (H_2, Zn, Co, Fe) for the fabrication of a series of carbon materials [215]. Among these materials, CPM-99Fe-derived catalyst exhibited the highest ORR activity due to the high porosity, rich N sources, coupled with uniformly dispersed FeN_x sites. Jiang and co-workers employed a metalloporphyrinic MOF, PCN-224–FeCo, with adjustable molar ratio of Fe^{II}/Co^{II} embedded in the center of the porphyrin ring, as precursors for the synthesis of FeCo–N-doped porous carbon (denoted as FeCo–NPC) [216]. The M–N_x species with different metals endows FeCo–NPC with particular activity and the optimized $FeCo_2$–NPC-900 demonstrated prominent catalytic performance with half-wave potential of 0.87 V, exceeding those of benchmark Pt/C and most of the reported non-precious metal catalysts.

5.2. Hydrogen evolution reaction

Hydrogen, emerging as a low carbon or zero carbon energy, is recognized as one of clean and green energy sources. At present, one of the most attractive options is to split renewable water into hydrogen, which can be stored and then oxidized (by burning in air or in a fuel cell) to release energy and regenerate water. Electrochemical methods are regarded as efficient and scalable means to realize this conversion. The electrochemical water-splitting process includes two half-reactions: HER and OER. Given that the water splitting needs high activation energy and large overpotential, high-performance electrocatalysts with low cost are highly desired to enhance the performance of electrocatalytic water splitting. In recent years, MOF-derived materials, including first row transition metals (or their alloys) and their oxides, phosphides and nitrides [79,85,95,217–222], have been intensively demonstrated as promising electrocatalysts for HER, potentially replacing currently best-known Pt-based materials.

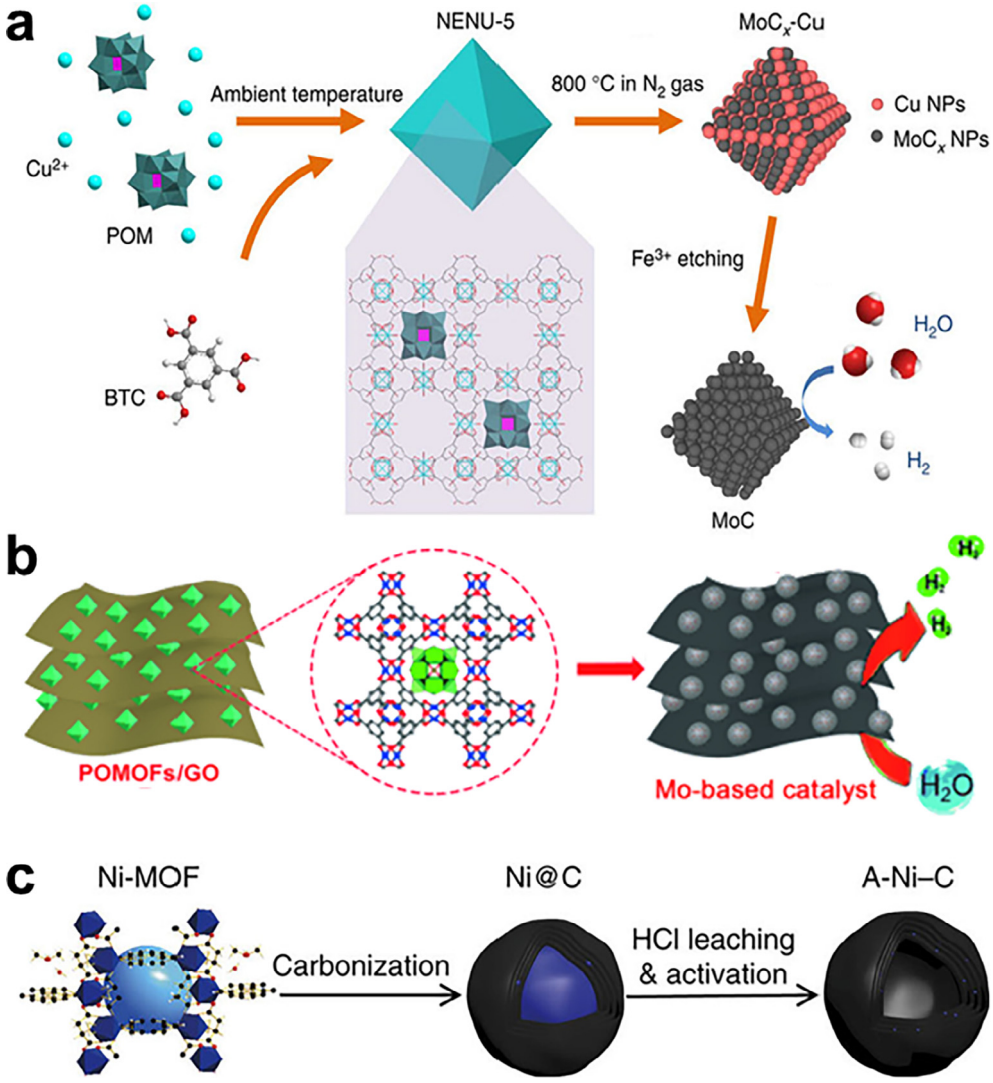

Fig. 9. (a) The synthetic procedure for porous MoC_x nano-octahedra. Adapted with permission from Ref. [85]. Copyright 2015, Nature Publishing Group. (b) Synthesis of porous MoO_2@PC–RGO catalyst. Adapted with permission from Ref. [221]. Copyright 2015, Wiley-VCH. (c) The synthetic procedure for A–Ni–C catalyst. Reproduced with permission from Ref. [222]. Copyright 2016, Nature Publishing Group.

Transition metal NPs are considered to be appropriate candidates for HER. Hou et al. prepared Co NPs embedded in the N-doped porous carbon polyhedra (denoted as N/Co-doped PCP//NRGO) through the pyrolysis of ZIF-67/GO composite [217]. The N/Co-doped PCP//NRGO showed excellent HER performance with a current density of 10 mA cm^{-2} at 229 mV in acid media, comparable to that of Pt/C. Xu et al. synthesized Ni NPs embedded in the N-doped graphene by carbonizing Ni–MOF (Ni_2–$(bdc)_2$ted) under N_2 atmosphere [218]. The optimized catalyst exhibited good HER activity, with a current density of 10 mA cm^{-2} at 205 mV, under alkaline conditions.

Transition metal phosphides/sulfides (TMP/TMS) have also been demonstrated as excellent electrocatalysts for HER. Zou and coworkers developed a bottom-up strategy to prepare CoP architecture encapsulated into BCN nanotubes (CoP@BCN) through a facile pyrolysis followed by phosphidation process of Co–MOF [220]. CoP@BCN-1 nanotubes exhibited the overpotential of 87 mV and 215 mV *vs* RHE at 10 mA cm^{-2} in 0.5 M H_2SO_4 and 0.1 M KOH, respectively. Lou's group prepared cubic NiS nanoframes via a reaction of Ni–Co PBA in the presence of S^{2-} at elevated temperature [95]. The resultant NiS with hollow nanostructure maintained the original cubic shape of pristine Ni–Co PBA and showed remarkable electrocatalytic activity and excellent durability for HER in alkaline solution.

In addition to the direct treatment and decoration of MOFs, the introduction of guest functional species into the cavities of MOFs has also been adopted for the synthesis of outstanding HER catalyst. Transition metal carbides, such as tungsten (W) and molybdenum (Mo) carbides have proven their great potential for decades in the fields of electrocatalysis in HER due to their inexpensive, excellent electrochemical performance and corrosion resistance. Wu et al. developed a novel MoC_x octahedral NPs through the pyrolysis of $H_3PMo_{12}O_{40}$ encapsulated in the cavities of NENU-5 (Fig. 9a) [85]. The obtained MoC_x-based catalyst exhibited remarkable electrocatalytic activity and stability for the HER. The superior electrocatalytic activity and good stability of MoC_x-based catalyst were mainly attributed to its porous and robust structure, ultrafine primary nanocrystallites and the synergistic effect between the MoC_x nanocrystallites and *in situ* incorporated carbon matrix. Given that decreased sizes of metal carbides would contribute to the enhancement of catalytic activity, Xu et al. synthesized small (*ca.* 2 nm) WC NPs through pyrolysis of MAF-6 encapsulating $W(CO)_6$ under N_2

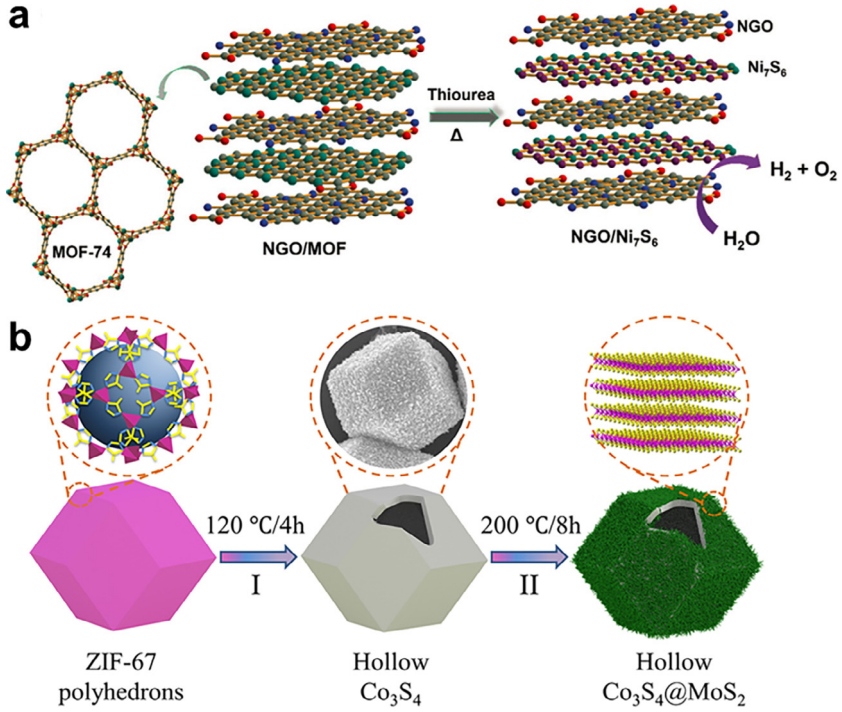

Fig. 10. (a) Synthesis of 2D NGO and nickel sulfide (NGO/Ni_7S_6) derived from MOF-74 using thiourea as a sulfur source under solvothermal conditions. Reproduced with permission from Ref. [225]. Copyright 2017, Wiley-VCH. (b) Schematic illustration of the formation of hollow Co_3S_4@MoS_2 heterostructures. Reproduced with the permission from Ref. [226]. Copyright 2017, American Chemical Society.

atmosphere at 980 °C [79]. Accordingly, the obtained catalyst exhibited superior HER activity with an overpotential of 51 mV at 10 mA cm^{-2}.

Considering the good electrical conductivity and high stability of MoO_2, Lan, Yu and co-workers developed porous MoO_2@PC–RGO as highly effective HER catalyst relying on the derivation of Cu-based MOF composites (Fig. 9b) [221]. In the synthetic procedures, NENU-5/GO composites (denoted as POMOFs/GO) were synthesized and underwent pyrolysis at 800 °C under N_2 atmosphere for 3 h. The porous MoO_2@PC–RGO catalysts were finally obtained by acid leaching for the removal of Cu NPs. The obtained MoO_2@-PC-RGO showed excellent HER activity with a very positive onset and low Tafel slope (41 mV/dec) in 0.5 M H_2SO_4, which is associated with the improved electrical conductivity induced by RGO nanosheets, the unique structure of MOF-derived porous materials (preventing the aggregation of MoO_2 NPs), and the doping of phosphorus (originating from MOF precursors).

Supported atomically dispersed catalysts have been investigated for the improvement of HER performance. Fan et al. developed a novel catalyst with atomically dispersed Ni species embedded in the carbon matrix through pyrolysis of Ni–MOF and subsequent acid leaching (for the removal of Ni NPs) (Fig. 9c) [222]. The single Ni atoms anchored on the graphitized carbons contributed greatly to HER performance. After HCl treatment, the activated A–Ni–C catalyst exhibited a very low overpotential (−34 mV) at the current density of 10 mA cm^{-2} and a large exchange current density of 1.2 mA cm^{-2} in 0.5 M H_2SO_4.

5.3. Oxygen evolution reaction

The OER has been viewed as a paramount reaction involved in the field of renewable energy such as metal–air batteries, which requires high-performance electrocatalysts to overcome the slow kinetics (involving multistep electron transfer). Nowadays the OER electrocatalysts mostly rely on noble-metal-based oxides (RuO_2 and IrO_2), suffering from high cost and low stability. Therefore, the pursuit of promising substitutes is a matter of urgency. Given that transition metals and their compounds hold great promise for replacing noble-metal-based oxides, MOFs and their composites are considered to be suitable precursors for preparing highly efficient OER catalysts [223–227].

TMP are well-known OER catalysts through the transformation under OER testing conditions. Lou's group developed a novel MOF-based strategy to synthesize Ni–Co bimetallic phosphide nanoboxes (denoted as NiCoP/C) through chemical conversion of Ni–Co layered double hydroxide (LDH) on the surface of ZIF-67 nanocubes (ZIF-67@LDH nanoboxes) formed by the subsequent reaction of $Ni(NO_3)_2$ with ZIF-67 nanocubes [223]. The NiCoP/C nanoboxes with hollow nanostructures performed better electrocatalytic activity and long-term stability for OER than those of Ni–Co layered double hydroxide (Ni–Co LDH) and Ni–Co mixed metal phosphide nanoboxes. Jiang and co-workers used another metalloporphyrinic MOF, PCN-600–Ni, integrated with GO, to provide an ideal precursor and template to fabricate bimetallic Fe–Ni phosphide/reduced graphene oxide composite via simple pyrolysis and subsequent phosphorization process [224]. Taking advantages of their highly ordered porosity, the synergetic effect of Fe and Ni species in bimetallic phosphide and the good conductivity of rGO, the optimized Fe–Ni–P/rGO-400 showed remarkable OER activity in 1 M KOH solution, realizing an extremely low overpotential of 240 mV at 10 mA cm^{-2}.

Transition metal sulfides have been broadly studied for OER. Among myriads of the species, nickel sulfide and cobalt sulfide have been identified as promising candidates for water splitting compared with iron, copper and tungsten sulfides. Recently, Schuhmann, Fischer and co-workers reported a facile, rational and effective method to fabricate a hybrid of N-doped graphene oxide/nickel sulfide nanosheets (denoted NGO/Ni_7S_6) from thermal annealing of a composite of a Ni–MOF stabilized on NGO layers (NGO/MOF) (Fig. 10a) [225]. The resultant NGO/Ni_7S_6 catalyst

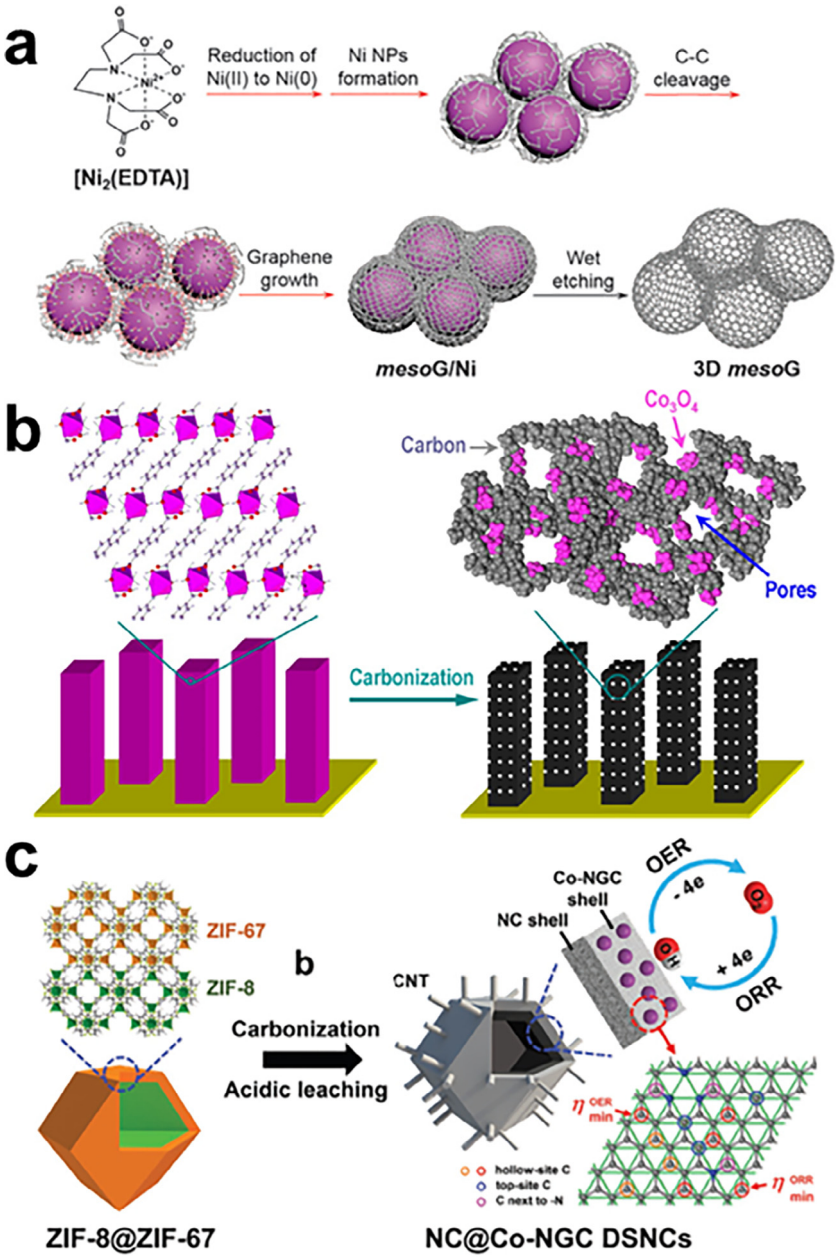

Fig. 11. (a) Synthetic route for the 3D mesoporous graphene. Reproduced with the permission from Ref. [228]. Copyright 2015, The Royal Society of Chemistry. (b) Schematic illustration for the preparation of Co_3O_4–C nanowire arrays. Reproduced with permission from Ref. [93]. Copyright 2014, American Chemical Society. (c) Synthesis of NC@Co–NGC DSNCs derived from ZIF-8@ZIF-67. Adapted with permission from Ref. [230]. Copyright 2017, Wiley-VCH.

needed 0.37 V to reach a current density of 10 mA cm^{-2}. The superior electrocatalytic activity and outstanding stability of NGO/Ni_7S_6 were mainly attributed to the hierarchical porous structure, enriched N and the synergistic effect between the Ni_7S_6 and NGO. Very recently, Yamauchi and co-workers successfully built core–shell Co_3S_4@MoS_2 heterostructure based on ZIF-67 (Fig. 10b) [226]. As expected, the obtained hollow Co_3S_4@MoS_2 exhibited obviously enhanced OER activity with an overpotential of 330 mV at 10 mA cm^{-2} in 1 M KOH. This novel preparation method will be very attractive for the fabrication of other hollow, multiple-component and highly effective nanocatalysts.

Considering that the agglomeration of MOFs during heat treatment may influence the performance of the catalyst. In view of this, Lu et al. synthesized 3D porous $CoFe_2O_4$/C nanoarrays with uniform distribution of carbon supported on NF by simple pyrolysis of bimetallic MOF hybrid, MOF-74–Co/Fe nanorod arrays on NF [227]. As expected, the resultant $CoFe_2O_4$/C NRAs catalyst performed excellent OER activity (1.47 V *vs* RHE at 10 mA cm^{-2}) and durability (only about 7.5% potential reduction at 100 mA cm^{-2} for 60 h).

5.4. Bifunctional electrocatalysis

Apart from the realization of single half reaction in the electrocatalysis process, a certain number of catalysts also show bifunctions in both OER and ORR, which is significant for many energy devices, particularly metal–air batteries. It is essential to develop bifunctional electrocatalysts since the integration of two different catalysts into metal–air batteries would make them complicated and hard to maintain, let alone the unfavorable volumetric energy density. Therefore, electrocatalysts possessing both ORR and OER activities should be appealing [93,228–230].

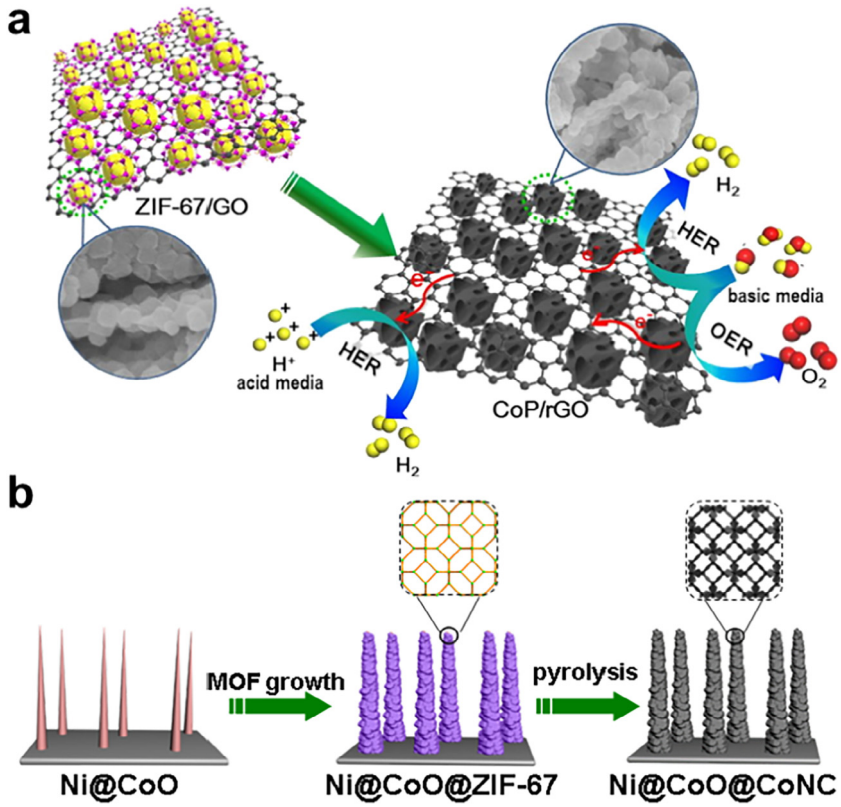

Fig. 12. (a) Schematic illustration for the construction of CoP/rGO from ZIF-67/GO composite for electrocatalytic water splitting. Reproduced with the permission from Ref. [92]. Copyright 2016, The Royal Society of Chemistry. (b) The fabrication of metal oxide@MOF hybrid arrays and their derived metal oxide@MOFC arrays on the 3D conductive matrix. Adapted with permission from Ref. [94]. Copyright 2017, Elsevier.

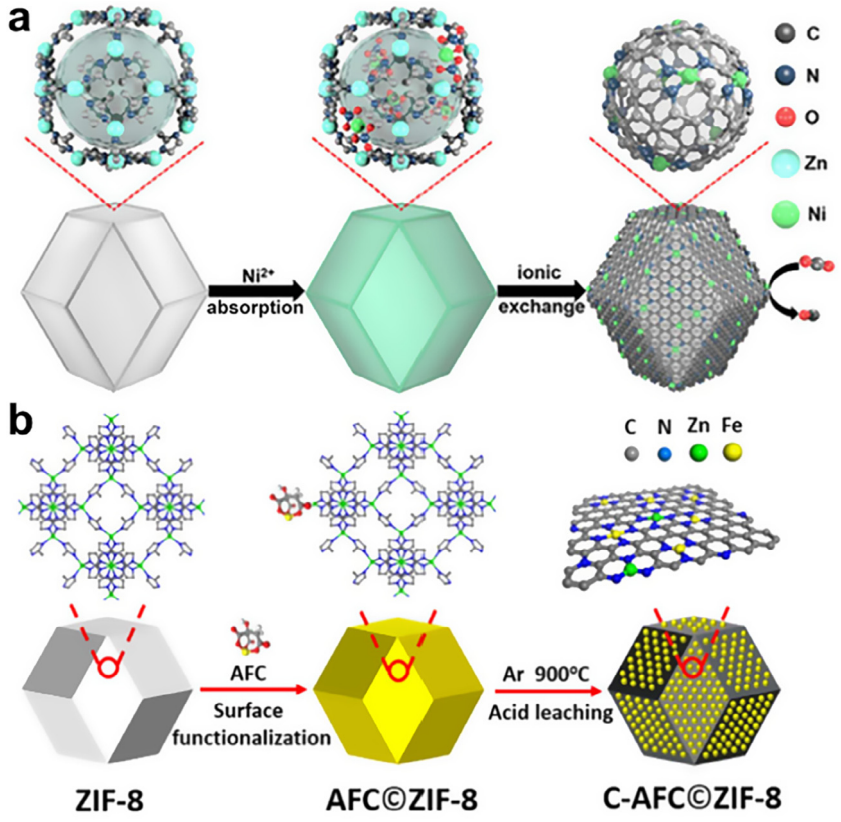

Fig. 13. (a) The formation of Ni SAs/N–C based on ZIF-8. Reproduced with permission from Ref. [233]. Copyright 2017, American Chemical Society. (b) Highly exposed Fe–N sites on the carbon matrix generated from ZIF-8. Reproduced with permission from Ref. [83]. Copyright 2017, Elsevier.

Lee et al. fabricated 3D mesoporous graphene through the simple pyrolysis of the [Ni_2(EDTA)] precursor under N_2 atmosphere for 1 h and subsequent wet etching to remove Ni NPs (Fig. 11a) [228]. The catalyst exhibited high OER activity, with a current density of 10 mA cm^{-2} at 1.56 V in 0.1 M KOH. In the ORR, the catalyst afforded a current density of −3 mA cm^{-2} at 0.76 V. The excellent OER and ORR performances can be assigned to the large surface area and the existence of active species (nickel and nitrogen). Qiao and co-workers developed a versatile strategy for the controllable preparation of hybrid porous nanowire arrays composed of Co_3O_4 and carbon by a facile carbonization of Co–MOF hybrid arrays grown on Cu foil (Fig. 11b) [93]. The resultant hybrid material exhibited superior activity for OER, with a low onset potential of 1.47 V *vs* RHE in 0.1 M KOH, affording a stable current density of 10.0 mA cm^{-2} at 1.52 V *vs* RHE. In the ORR, the catalyst reached a half-wave potential of 0.78 V. The excellent performances of the catalyst were mainly attributed to the integrated hierarchical pores and the synergistic advantages between the metal oxide core and the conductive substrate. In addition, Qiu, Zhao and co-workers synthesized double-shelled hybrid nanocages with Co–N-doped graphitic carbon (Co–NGC) as shell and N-doped microporous carbon (NC) as core by templating ZIF-8@ZIF-67 core–shell bimetallic MOFs (Fig. 11c) [230]. The resultant NC@Co–NGC DSNCs were then applied as an active and stable electrocatalyst for ORR, with a half-wave potential of 0.82 V in 0.1 M KOH. In the OER, the catalyst can reach a current density of 10 mA cm^{-2} at 1.64 V under the same condition.

The integration of OER and HER functionalities into a single electrocatalyst to realize the overall water splitting is highly desired as well. In recent years, a number of MOF-derived porous composites, especially transition metal phosphides/sulfides/selenides, have been widely investigated for electrocatalytic water splitting. Jiang and co-workers successfully synthesized a series of layered CoP/rGO composites by the pyrolysis of sandwich-type ZIF-67/GO, followed by subsequent phosphating process (Fig. 12a) [92]. The optimized CoP/rGO-400 exhibited excellent HER activity in a wide pH range of 0–14 with overpotentials of 105 mV in acidic conditions and 150 mV in basic electrolyte at 10 mA cm^{-2}. Furthermore, it also displayed enhanced OER activity in basic solution with an overpotential of 340 mV at 10 mA cm^{-2}. When performed as a bifunctional electrocatalyst for overall water splitting, CoP/rGO-400 shows superior activity to the integrated Pt/C and IrO_2 couple.

In a later publication, Cai et al. developed a general self-sacrificing template strategy for the successful fabrication of metal oxide@MOF or metal hydroxide@MOF hybrid arrays on various substrates (Fig. 12b) [94]. Taking the preparation of Ni@CoO@MOFC as a representative, conductive substrates (Ni foil) were first utilized for the growth of CoO nanowire arrays. Then these arrays were acted as self-sacrificial templates for the fabrication of ZIF-67. Remarkably, after facile pyrolysis under N_2 atmosphere, the resultant Ni@CoO@MOFC showed hierarchical pores and exhibited high HER (190 mV at a current density of 10 mA cm^{-2}) and OER (309 mV at a current density of 10 mA cm^{-2}) electrocatalytic activity. The high performance of Ni@CoO@MOFC can be assigned to the unique configuration of nanoarrays, as mentioned above, and the hierarchically porous structure.

Guan et al. also reported a kind of hollow CoS_2 nanotube arrays stabilized on a carbon cloth substrate (denoted CoS_2 NTA/CC) via a simple sulfidation process of Co–MOF arrays [231]. The obtained CoS_2 NTA/CC catalyst showed comparable properties to many other reported non-precious electrocatalyst for overall water splitting in alkaline media, realizing small overpotentials in HER (193 mV at 10 mA cm^{-2}) and OER (276 mV at 10 mA cm^{-2}).

5.5. Alcohol oxidation, CO_2 reduction and others

In addition to electrocatalytic ORR, HER and OER described above, other electrocatalytic reactions such as MOR, CO_2RR and organic reactions have also been conducted over MOF-derived catalysts. Direct methanol fuel cells, with high energy density, the ease of availability and low cost, have attracted intensive attention. Xu's group reported hierarchically porous carbons with both micro- and mesopores generated by pyrolysis of ZIF-8 as supports for Pd NPs [232]. The obtained Pd/ZC-1000 catalyst showed high MOR performance under alkaline conditions because of the high surface area (1105 m^2 g^{-1}), large pore volume (0.95 cm^3 g^{-1}) and high graphitic degree. Furthermore, the electrocatalytic MOR activity of Pd/ZC-1000 is 5 times higher than that of Pd/XC-72R at the same Pd loading.

Electrochemical CO_2RR, as another effective strategy to produce value-added products, has aroused widespread concern. The decrease of large overpotential for electron transfer from the catalysts to CO_2 and the competition between HER and CO_2RR are still major challenges for the development of CO_2RR. Recently, Zhao et al. adopted MOF assisted strategy for the synthesis of single nickel atoms dispersed in N-doped porous carbon (denoted as Ni SAs/N–C) via pyrolysis of $Ni(NO_3)_2$@ZIF-8 composites (Fig. 13a) [233]. As expected, the resultant Ni SAs/N–C exhibited clearly improved CO_2 reduction performance, with high Faradaic efficiency to CO (over 70%) at −0.9 V *vs* RHE and excellent TOF (5273 h^{-1}), outperforming those of Ni NPs/N–C and most of previous catalysts. Ye et al. selectively confined ammonium ferric citrate (AFC) to ZIF-8 framework by adopting post-synthetic modification strategy and then isolated Fe–N sites located carbons (denoted as AFC@ZIF-8) were generated through pyrolysis (Fig. 13b) [83]. The highly exposed Fe–N sites demonstrated superior mass activity and selectivity toward CO_2RR, outperforming most of previous non-noble metal catalysts.

The N-methylation and N,N-dimethylation reactions are of importance for preparing many intermediates or valuable products such as pesticides, dyes and perfumes in chemical industry. Previous reports demonstrated that using CO_2 as C1 resource is an effective route to synthesize N,N-dimethylanilines. However, direct N-methylation of nitrobenzenes was generally studied using H_2 or $PhSiH_3$ as reducing agent under harsh conditions such as high temperature or/and high pressure. Han and co-workers designed a novel electrocatalyst Pd/Co–N/carbon using ZIF-8 as precursor by the carbonization of the Co–ZIF/graphene oxide (GO) at 800 °C under argon atmosphere followed by the immobilization of Pd NPs [234]. The electrocatalytic N-methylation of nitrobenzenes was conducted efficiently under ambient reaction conditions with high yields of the desired product, which was mainly accelerated by the Pd/Co–N/carbon as electrocatalyst and 1-amino-methylphosphonic acid (AMPA) as thermal co-catalyst.

6. Conclusions and prospects

In summary, though in an early stage, MOFs have been demonstrated to be ideal templates/precursors for the fabrication of various carbon- or metal-based porous materials, as demonstrated by the available reports. Various synthetic strategies have also been developed to prepare MOF-derived porous materials, such as thermal transformation, solution infiltration method followed by heat treatment and so on. Quite a few derivatives based on MOFs have been reported, including metal-free carbons, metal-based compounds (metal oxides/carbides/nitrides/sulfides/phosphides, etc.) and their composites, greatly enriching the family of porous materials. When performed as catalysts, MOF-derived porous materials

show superior performances in all heterogeneous organocatalysis, photocatalysis and electrocatalysis.

Inheriting the remarkable features of pristine MOFs to a great extent, MOF-derived porous materials present many advantages: (a) uncomplicated preparation procedure, generally through a direct pyrolysis from MOFs or MOF composites; (b) morphology and pore size (partially) inherited from pristine MOFs; (c) hierarchically porous structure, guaranteeing the accessibility of active sites and efficient mass transfer during catalytic processes; (d) large surface areas, favoring the high dispersion of active sites, adsorption and enrichment of reactant molecules around the active sites; (e) easy doping of heteroatoms, from MOF precursors or guest species, providing necessary compositions for catalysis; and others.

In addition, some MOF-derived composites with specific structures possess unique advantages. The introduction of the substrates (NF, GO, etc.) during the catalyst fabrication can greatly modulate the conductivity of MOF-derived porous materials, which is of particular significance for electrocatalysis. Furthermore, as mentioned above, the nanoarrays supported on the conductive substrates further contribute to mass transfer, increasing the utilization of active sites. The unique structure also avoids the peeling off the catalysts during the release of gas bubbles. To sum up, the enhancement of the catalytic performance lies in valid active sites, efficient mass transfer and excellent stability of the matrix, all of which can be graciously realized with MOF-derived porous materials, upon rational design and fabrication.

Though amazing advances have been achieved, MOF-derived porous materials are still in their infancy currently and some underdeveloped issues are still needed to be solved: (a) Limited choices of MOF precursors. Although more than 20,000 MOFs have been reported, only a few MOFs have been chosen as proper precursors and more alternative MOFs should be explored. (b) The price and large-scale preparation of MOF precursors. To promote basic research to practical industrialization, the low-cost MOF precursor should be prepared in a large scale. (c) Accurate control over the pore structures of MOF-derived composites. The pyrolysis usually requires high temperatures, which puts an obstacle in rationally controlled synthesis of MOF-derived materials with desired pore character. (d) Precise control over the active sites. Despite the excellent performance of MOF-derived porous materials, they always suffer from multiphase due to the hardly controllable derivation methods. Therefore, more intensive efforts should be devoted to the design and control on the active species, which can help to better understand the reaction mechanism. (e) Unawareness of the transformation process from MOFs to their derivatives, due to the lack of *in situ* (operando) techniques to track MOF evolution mechanism at high temperatures. To realize the synthesis of target functional materials and have a profound understanding of the formation mechanism of MOF-derived materials, it is crucial to realize the monitoring of the evolution of MOFs during pyrolysis through *in situ* (operando) techniques, which will shed light on the rational design and synthesis of MOF-derived porous materials.

Aside from the functional design of MOF-based precursors, in-depth understanding of structure–property relationship from the viewpoint of fundamental research is also highly desired. Meanwhile, more attentions should also be paid to important reactions associated with energy storage/conversion as well as the synthesis of high value-added products. Given the unparalleled features including high surface area, large porosity, abundant active species, flexible tailorability and tunable porous structure, we believe that the MOF-derived porous materials will present a bright future toward catalysis.

Acknowledgements

This work was supported by the NSFC (21725101, 21673213, 21521001 and 21701093) the National Research Fund for Fundamental Key Project (2014CB931803), and the NSF of Shandong Province (ZR201702200574).

References

[1] K. Kim, T. Lee, Y. Kwon, Y. Seo, J. Song, J.K. Park, H. Lee, J.Y. Park, H. Ihee, S.J. Cho, R. Ryoo, Nature 535 (2016) 131–135.
[2] J. Zhang, L. Wang, Y. Shao, Y. Wang, B.C. Gates, F.-S. Xiao, Angew. Chem., Int. Ed. 56 (2017) 9747–9751.
[3] M. Hartmann, A.G. Machoke, W. Schwieger, Chem. Soc. Rev. 45 (2016) 3313–3330.
[4] C. Wang, L. Wang, J. Zhang, H. Wang, J.P. Lewis, F.-S. Xiao, J. Am. Chem. Soc. 138 (2016) 7880–7883.
[5] J. Kim, H.R. Cho, H. Jeon, D. Kim, C. Song, N. Lee, S.H. Choi, T. Hyeon, J. Am. Chem. Soc. 139 (2017) 10992–10995.
[6] B. Ruehle, D.L. Clemens, B.-Y. Lee, M.A. Horwitz, J.I. Zink, J. Am. Chem. Soc. 139 (2017) 6663–6668.
[7] Y. Sun, K. Ma, T. Kao, K.A. Spoth, H. Sai, D. Zhang, L.F. Kourkoutis, V. Elser, U. Wiesner, Nat. Commun. 8 (2017) 252.
[8] W.J. Roth, P. Nachtigall, R.E. Morris, J. Čejka, Chem. Rev. 114 (2014) 4807–4837.
[9] B.M. Weckhuysen, J. Yu, Chem. Soc. Rev. 44 (2015) 7022–7024.
[10] J. Liang, Z. Liang, R. Zou, Y. Zhao, Adv. Mater. 29 (2017) 1701139.
[11] J. Wen, K. Yang, F. Liu, H. Li, Y. Xu, S. Sun, Chem. Soc. Rev. 46 (2017) 6024–6045.
[12] W. Li, J. Liu, D. Zhao, Nat. Rev. Mater. 1 (2016) 16023.
[13] J. Wei, Z. Sun, W. Luo, Y. Li, A.A. Elzatahry, A.M. Al-Enizi, Y. Deng, D. Zhao, J. Am. Chem. Soc. 139 (2017) 1706–1713.
[14] L.J. Murray, M. Dincă, J.R. Long, Chem. Soc. Rev. 38 (2009) 1294–1314.
[15] J. Li, Y. Ma, M.C. McCarthy, J. Sculley, J. Yu, H.-K. Jeong, P.B. Balbuena, H.-C. Zhou, Coord. Chem. Rev. 255 (2011) 1791–1823.
[16] J.Y. Kim, R. Balderas-Xicohtencatl, L. Zhang, S.G. Kang, M. Hirscher, H. Oh, H.R. Moon, J. Am. Chem. Soc. 139 (2017) 15135–15141.
[17] Q. Xia, Z. Li, C. Tan, Y. Liu, W. Gong, Y. Cui, J. Am. Chem. Soc. 139 (2017) 8259–8266.
[18] G. Huang, Q. Yang, Q. Xu, S.-H. Yu, H.-L. Jiang, Angew. Chem., Int. Ed. 55 (2016) 7379–7383.
[19] T. Islamoglu, S. Goswami, Z. Li, A.J. Howarth, O.K. Farha, J.T. Hupp, Acc. Chem. Res. 50 (2017) 805–813.
[20] A.H. Chughtai, N. Ahmad, H.A. Younus, A. Laypkov, F. Verpoort, Chem. Soc. Rev. 44 (2015) 6804–6849.
[21] B. Li, M. Chrzanowski, Y. Zhang, S. Ma, Coord. Chem. Rev. 307 (2016) 106–129.
[22] X. Yu, S.M. Cohen, J. Am. Chem. Soc. 138 (2016) 12320–12323.
[23] H.R. Moon, D.-W. Limb, M.P. Suh, Chem. Soc. Rev. 42 (2013) 1807–1824.
[24] C.R. Kim, T. Uemura, S. Kitagawa, Chem. Soc. Rev. 45 (2016) 3828–3845.
[25] M. Zhao, K. Yuan, Y. Wang, G. Li, J. Guo, L. Gu, W. Hu, H. Zhao, Z. Tang, Nature 539 (2016) 76–80.
[26] Q. Yang, Q. Xu, S.-H. Yu, H.-L. Jiang, Angew. Chem., Int. Ed. 55 (2016) 3685–3689.
[27] Y.-Z. Chen, Z.U. Wang, H. Wang, J. Lu, S.-H. Yu, H.-L. Jiang, J. Am. Chem. Soc. 139 (2017) 2035–2044.
[28] C.-D. Wu, M. Zhao, Adv. Mater. 29 (2017) 1605446.
[29] R.-B. Lin, F. Li, S.-Y. Liu, X.-L. Qi, J.-P. Zhang, X.-M. Chen, Angew. Chem., Int. Ed. 52 (2013) 13429–13433.
[30] W.P. Lustig, S. Mukherjee, N.D. Rudd, A.V. Desai, J. Li, S.K. Ghosh, Chem. Soc. Rev. 46 (2017) 3242–3285.
[31] F.-Y. Yi, D. Chen, M.-K. Wu, L. Han, H.-L. Jiang, ChemPlusChem 81 (2016) 675–690.
[32] J.-K. Sun, Q. Xu, Energy Environ. Sci. 7 (2014) 2071–2100.
[33] H. Wang, Q.-L. Zhu, R. Zou, Q. Xu, Chem 2 (2017) 52–80.
[34] S.-N. Zhao, X.-Z. Song, S.-Y. Song, H.-J. Zhang, Coord. Chem. Rev. 337 (2017) 80–96.
[35] Q. Yang, Q. Xu, H.-L. Jiang, Chem. Soc. Rev. 46 (2017) 4774–4808.
[36] J. Liu, L. Chen, H. Cui, J. Zhang, L. Zhang, C.-Y. Su, Chem. Soc. Rev. 43 (2014) 6011–6061.
[37] G. Huang, Y.-Z. Chen, H.-L. Jiang, Acta Chim. Sinica 74 (2016) 113–129.
[38] L. Jiao, Y. Wang, H.-L. Jiang, Q. Xu, Adv. Mater. 29 (2017) 1703663.
[39] W. Zhang, Y. Hu, J. Ge, H.-L. Jiang, S.-H. Yu, J. Am. Chem. Soc. 136 (2014) 16978–16981.
[40] T. Zhang, W. Lin, Chem. Soc. Rev. 43 (2014) 5982–5993.
[41] J.-S. Qin, D.-Y. Du, W. Guan, X.-J. Bo, Y.-F. Li, L.-P. Guo, Z.-M. Su, Y.-Y. Wang, Y.-Q. Lan, H.-C. Zhou, J. Am. Chem. Soc. 137 (2015) 7169–7177.
[42] S. Zhao, Y. Wang, J. Dong, C.-T. He, H. Yin, P. An, K. Zhao, X. Zhang, C. Gao, L. Zhang, J. Lv, J. Wang, J. Zhang, A.M. Khattak, N.A. Khan, Z. Wei, J. Zhang, S. Liu, H. Zhao, Z. Tang, Nat. Energy 1 (2016) 16184.
[43] K.J. Lee, J.H. Lee, S. Jeoung, H.R. Moon, Acc. Chem. Res. 50 (2017) 2684–2692.
[44] X. Cao, C. Tan, M. Sindoro, H. Zhang, Chem. Soc. Rev. 46 (2017) 2660–2677.
[45] S. Dang, Q.-L. Zhu, Q. Xu, Nat. Rev. Mater. 3 (2017) 17075.
[46] H.B. Wu, X.-W. Lou, Sci. Adv. 3 (2017) eaap9252.

[47] L. Yang, X. Zeng, W. Wang, D. Cao, Adv. Funct. Mater. 28 (2018) 1704537, https://doi.org/10.1002/adfm.201704537.
[48] L. Lux, K. Williams, S. Ma, CrystEngComm 17 (2015) 10–22.
[49] J. Tang, R.R. Salunkhe, J. Liu, N.L. Torad, M. Imura, S. Furukawa, Y. Yamauchi, J. Am. Chem. Soc. 137 (2015) 1572–1580.
[50] K. Shen, X. Chen, J. Chen, Y. Li, ACS Catal. 6 (2016) 5887–5903.
[51] Z. Song, N. Cheng, A. Lushington, X. Sun, Catalysts 6 (2016) 116–134.
[52] L. Oar-Arteta, T. Wezendonk, X. Sun, F. Kapteijn, J. Gascon, Mater. Chem. Front. 1 (2017) 1709–1745.
[53] Y.V. Kaneti, J. Tang, R.R. Salunkhe, X. Jiang, A. Yu, K.C.-W. Wu, Y. Yamauchi, Adv. Mater. 29 (2017) 1604898.
[54] W. Xia, A. Mahmood, R. Zou, Q. Xu, Energy Environ. Sci. 8 (2015) 1837–1866.
[55] M.H. Yap, K.L. Fow, G.Z. Chen, Green Energy Environ. 2 (2017) 218–245.
[56] S. Fu, C. Zhu, J. Song, D. Du, Y. Lin, Adv. Energy Mater. 7 (2017) 1700363.
[57] J. Wang, F. Xu, H. Jin, Y. Chen, Y. Wang, Adv. Mater. 29 (2017) 1605838.
[58] H.D. Mai, K. Rafiq, H. Yoo, Chem. Eur. J. 23 (2017) 5631–5651.
[59] Y. Qian, I.A. Khan, D. Zhao, Small 13 (2017) 1701143.
[60] Z. Liang, C. Qu, W. Guo, R. Zou, Q. Xu, Adv. Mater. 30 (2018), https://doi.org/10.1002/adma.201702891.
[61] A. Mahmood, W. Guo, H. Tabassum, R. Zou, Adv. Energy Mater. 6 (2016) 1600423.
[62] Z. Li, M. Shao, L. Zhou, R. Zhang, C. Zhang, M. Wei, D.G. Evans, X. Duan, Adv. Mater. 28 (2016) 2337–2344.
[63] T.K. Kim, K.J. Lee, J.Y. Cheon, J.H. Lee, S.H. Joo, H.R. Moon, J. Am. Chem. Soc. 135 (2013) 8940–8946.
[64] C. Zhang, Y.-C. Wang, B. An, R. Huang, C. Wang, Z. Zhou, W. Lin, Adv. Mater. 29 (2017) 1604556.
[65] S.J. Yang, S. Nam, T. Kim, J.H. Im, H. Jung, J.H. Kang, S. Wi, B. Park, C.R. Park, J. Am. Chem. Soc. 135 (2013) 7394–7397.
[66] H.-L. Jiang, B. Liu, Y.-Q. Lan, K. Kuratani, T. Akita, H. Shioyama, F. Zong, Q. Xu, J. Am. Chem. Soc. 133 (2011) 11854–11857.
[67] M. Hu, J. Reboul, S. Furukawa, N.L. Torad, Q. Ji, P. Srinivasu, K. Ariga, S. Kitagawa, Y. Yamauchi, J. Am. Chem. Soc. 134 (2012) 2864–2867.
[68] B. Liu, X. Zhang, H. Shioyama, T. Mukai, T. Sakai, Q. Xu, J. Power Sources 195 (2010) 857–861.
[69] R.R. Salunkhe, J. Tang, Y. Kamachi, T. Nakato, J.H. Kim, Y. Yamauchi, ACS Nano 9 (2015) 6288–6296.
[70] K. Khaletskaya, A. Pougin, R. Medishetty, C. Röler, C. Wiktor, J. Strunk, R.A. Fischer, Chem. Mater. 27 (2015) 7248–7257.
[71] W. Cho, S. Park, M. Oh, Chem. Commun. 47 (2011) 4138–4140.
[72] A. Banerjee, U. Singh, V. Aravindan, M. Srinivasan, S. Ogale, Nano Energy 2 (2013) 1158–1163.
[73] L. Hu, N. Yan, Q. Chen, P. Zhang, H. Zhong, X. Zheng, Y. Li, X. Hu, Chem. Eur. J. 18 (2012) 8971–8977.
[74] C. Li, T. Chen, W. Xu, X. Lou, L. Pan, Q. Chen, B. Hu, J. Mater. Chem. A 3 (2015) 5585–5591.
[75] X. Xu, R. Cao, S. Jeong, J. Cho, Nano Lett. 12 (2012) 4988–4991.
[76] C. Wei, X. Li, F. Xu, H. Tan, Z. Li, L. Sun, Y. Song, Anal. Methods 6 (2014) 1550–1557.
[77] J. Ma, H. Wang, X. Yang, Y. Chai, R. Yuan, J. Mater. Chem. A 3 (2015) 12038–12043.
[78] B. Liu, H. Shioyama, T. Akita, Q. Xu, J. Am. Chem. Soc. 130 (2008) 5390–5391.
[79] Y.-T. Xu, X. Xiao, Z.-M. Ye, S. Zhao, R. Shen, C.-T. He, J.-P. Zhang, Y. Li, X.-M. Chen, J. Am. Chem. Soc. 139 (2017) 5285–5288.
[80] Q. Lai, L. Zheng, Y. Liang, J. He, J. Zhao, J. Chen, ACS Catal. 7 (2017) 1655–1663.
[81] F. Cheng, W.-C. Li, J.-N. Zhu, W.-P. Zhang, A.-H. Lu, Nano Energy 19 (2016) 486–494.
[82] Q.-L. Zhu, W. Xia, T. Akita, R. Zou, Q. Xu, Adv. Mater. 28 (2016) 6391–6398.
[83] Y. Ye, F. Cai, H. Li, H. Wu, G. Wang, Y. Li, S. Miao, S. Xie, R. Si, J. Wang, X. Bao, Nano Energy 38 (2017) 281–289.
[84] A. Aijaz, N. Fujiwara, Q. Xu, J. Am. Chem. Soc. 136 (2014) 6790–6793.
[85] H. Wu, B. Xia, L. Yu, X.-Y. Yu, X.-W. Lou, Nat. Commun. 6 (2015) 6512.
[86] Y. Chen, S. Ji, Y. Wang, J. Dong, W. Chen, Z. Li, R. Shen, L. Zheng, Z. Zhuang, D. Wang, Y. Li, Angew. Chem., Int. Ed. 56 (2017) 6937–6941.
[87] C.D. Malonzo, S.M. Shaker, L. Ren, S.D. Prinslow, A.E. Platero-Prats, L.C. Gallington, J. Borycz, A.B. Thompson, T.C. Wang, O.K. Farha, J.T. Hupp, C.C. Lu, K.W. Chapman, J.C. Myers, R.L. Penn, L. Gagliardi, M. Tsapatsis, A. Stein, J. Am. Chem. Soc. 138 (2016) 2739–2748.
[88] Q.-L. Zhu, W. Xia, L.-R. Zheng, R. Zou, Z. Liu, Q. Xu, ACS Energy Lett. 2 (2017) 504–511.
[89] G. Huang, F. Zhang, X. Du, Y. Qin, D. Yin, L. Wang, ACS Nano 9 (2015) 1592–1599.
[90] H.-X. Zhong, J. Wang, Y.-W. Zhang, W.-L. Xu, W. Xing, D. Xu, Y.-F. Zhang, X.-B. Zhang, Angew. Chem., Int. Ed. 53 (2014) 14235–14239.
[91] G. Zhang, S. Hou, H. Zhang, W. Zeng, F. Yan, C.C. Li, H. Duan, Adv. Mater. 27 (2015) 2400–2405.
[92] L. Jiao, Y.-X. Zhou, H.-L. Jiang, Chem. Sci. 7 (2016) 1690–1695.
[93] T. Ma, S. Dai, M. Jaroniec, S. Qiao, J. Am. Chem. Soc. 136 (2014) 13925–13931.
[94] G. Cai, W. Zhang, L. Jiao, S.-H. Yu, H.-L. Jiang, Chem 2 (2017) 791–802.
[95] X.-Y. Yu, L. Yu, H.B. Wu, X.-W. Lou, Angew. Chem., Int. Ed. 54 (2015) 5331–5335.
[96] Z. Li, C. Li, X. Ge, J. Ma, Z. Zhang, Q. Li, C. Wang, L. Yin, Nano Energy 23 (2016) 15–26.
[97] K. Cho, S.-H. Han, M.P. Suh, Angew. Chem., Int. Ed. 55 (2016) 15301–15305.
[98] Z. Jiang, H. Sun, Z. Qin, X. Jiao, D. Chen, Chem. Commun. 48 (2012) 3620–3622.
[99] G. Yu, J. Sun, F. Muhammad, P. Wang, G. Zhu, RSC Adv. 4 (2014) 38804–38811.
[100] H. Tan, C. Ma, L. Gao, Q. Li, Y. Song, F. Xu, T. Wang, L. Wang, Chem. Eur. J. 20 (2014) 16377–16383.
[101] W. Zhong, H. Liu, C. Bai, S. Liao, Y. Li, ACS Catal. 5 (2015) 1850–1856.
[102] Y.-X. Zhou, Y.-Z. Chen, L. Cao, J. Lu, H.-L. Jiang, Chem. Commun. 51 (2015) 8292–8295.
[103] C. Bai, X. Yao, Y. Li, ACS Catal. 5 (2015) 884–891.
[104] X. Yao, C. Bai, J. Chen, Y. Li, RSC Adv. 6 (2016) 26921–26928.
[105] R. Fang, R. Luque, Y. Li, Green Chem. 18 (2016) 3152–3157.
[106] X. Wang, Y. Li, J. Mater. Chem. A 4 (2016) 5247–5257.
[107] S. Ji, Y. Chen, Q. Fu, Y. Chen, J. Dong, W. Chen, Z. Li, Y. Wang, L. Gu, W. He, C. Chen, Q. Peng, Y. Huang, X. Duan, D. Wang, C. Draxl, Y. Li, J. Am. Chem. Soc. 139 (2017) 9795–9798.
[108] C. Bai, A. Li, X. Yao, H. Liu, Y. Li, Green Chem. 18 (2016) 1061–1069.
[109] Y.-Z. Chen, G. Cai, Y. Wang, Q. Xu, S.-H. Yu, H.-L. Jiang, Green Chem. 18 (2016) 1212–1217.
[110] X. Wang, W. Chen, L. Zhang, T. Yao, W. Liu, Y. Lin, H. Ju, J. Dong, L. Zheng, W. Yan, X. Zheng, Z. Li, X. Wang, J. Yang, D. He, Y. Wang, Z. Deng, Y. Wu, Y. Li, J. Am. Chem. Soc. 139 (2017) 9419–9422.
[111] S. Ding, C. Zhang, Y. Liu, H. Jiang, W. Xing, R. Chen, J. Ind. Eng. Chem. 46 (2017) 258–265.
[112] J. Long, Y. Zhou, Y. Li, Chem. Commun. 51 (2015) 2331–2334.
[113] X. Liu, S. Cheng, J. Long, W. Zhang, X. Liu, D. Wei, Mater. Chem. Front. 1 (2017) 2005–2012.
[114] R.V. Jagadeesh, K. Murugesan, A.S. Alshammari, H. Neumann, M.-M. Pohl, J. Radnik, M. Beller, Science 358 (2017) 326–332.
[115] X. Li, C. Zeng, J. Jiang, L. Ai, J. Mater. Chem. A 4 (2016) 7476–7482.
[116] J. Long, K. Shen, Y. Li, ACS Catal. 7 (2017) 275–284.
[117] B. Tang, W.-C. Song, E.-C. Yang, X.-J. Zhao, RSC Adv. 7 (2017) 1531–1539.
[118] X. Kang, H. Liu, M. Hou, X. Sun, H. Han, T. Jiang, Z. Zhang, B. Han, Angew. Chem., Int. Ed. 55 (2016) 1080–1084.
[119] Y. Xu, X.-J. Lv, Y. Chen, W.-F. Fu, Catal. Commun. 101 (2017) 31–35.
[120] J. Long, K. Shen, L. Chen, Y. Li, J. Mater. Chem. A 4 (2016) 10254–10262.
[121] K. Shen, L. Chen, J. Long, W. Zhong, Y. Li, ACS Catal. 5 (2015) 5264–5271.
[122] H. Yang, S.J. Bradley, A. Chan, G.I.N. Waterhouse, T. Nann, P.E. Kruger, S.G. Telfer, J. Am. Chem. Soc. 138 (2016) (1881) 11872–11881.
[123] Y. Li, Y.-X. Zhou, X. Ma, H.-L. Jiang, Chem. Commun. 52 (2016) 4199–4202.
[124] X. Ma, Y.-X. Zhou, H. Liu, Y. Li, H.-L. Jiang, Chem. Commun. 52 (2016) 7719–7722.
[125] G. Huang, L. Yang, X. Ma, J. Jiang, S.-H. Yu, H.-L. Jiang, Chem. Eur. J. 22 (2016) 3470–3477.
[126] X. Li, B. Zhang, Y. Fang, W. Sun, Z. Qi, Y. Pei, S. Qi, P. Yuan, X. Luan, T.W. Goh, W. Huang, Chem. Eur. J. 23 (2017) 4266–4270.
[127] L. Foppa, J. Dupont, Chem. Soc. Rev. 44 (2015) 1886–1897.
[128] C. Vangelis, A. Bouriazos, S. Sotiriou, M. Samorski, B. Gutsche, G. Papadogianakis, J. Catal. 274 (2010) 21–28.
[129] Y. Gong, P. Zhang, X. Xu, Y. Li, H. Li, Y. Wang, J. Catal. 297 (2013) 272–280.
[130] T. Toyao, M. Fujiwaki, K. Miyahara, T.-H. Kim, Y. Horiuchi, M. Matsuoka, ChemSusChem 8 (2015) 3905–3912.
[131] M. Ding, S. Chen, X.-Q. Liu, L.-B. Sun, J. Lu, H.-L. Jiang, ChemSusChem 10 (2017) 1898–1903.
[132] M. Chen, D. Goodman, Science 306 (2004) 252–255.
[133] M. Haruta, Nature 437 (2005) 1098–1099.
[134] H.-L. Jiang, B. Liu, T. Akita, M. Haruta, H. Sakurai, Q. Xu, J. Am. Chem. Soc. 131 (2009) 11302–11303.
[135] M. Teng, L. Luo, X. Yang, Microporous Mesoporous Mater. 119 (2009) 158–164.
[136] F. Zhang, C. Chen, W.-M. Xiao, L. Xu, N. Zhang, Catal. Commun. 26 (2012) 25–29.
[137] S. Li, N. Wang, Y. Yue, G. Wang, Z. Zu, Y. Zhang, Chem. Sci. 6 (2015) 2495–2500.
[138] H. Liu, S. Zhang, Y. Liu, Z. Yang, X. Feng, X. Lu, F. Huo, Small 11 (2015) 3130–3134.
[139] S. Zhang, H. Liu, C. Sun, P. Liu, L. Li, Z. Yang, X. Feng, F. Huo, X. Lu, J. Mater. Chem. A 3 (2015) 5294–5298.
[140] R. Zhang, L. Hu, S. Bao, R. Li, L. Gao, R. Li, Q. Chen, J. Mater. Chem. A 4 (2016) 8412–8420.
[141] X. Wang, S. Zhao, Y. Zhang, Z. Wang, J. Feng, S. Song, H. Zhang, Chem. Sci. 7 (2016) 1109–1114.
[142] C. Zhu, T. Dong, W. Gao, K. Ma, Y. Tian, X. Li, Int. J. Hydrogen Energy 42 (2017) 17457–17465.
[143] X. Wang, W. Zhong, Y. Li, Catal. Sci. Technol. 5 (2015) 1014–1020.
[144] S. Abello, D. Montane, ChemSusChem 4 (2011) 1538–1556.
[145] E. de Smit, B.M. Weckhuysen, Chem. Soc. Rev. 37 (2008) 2758–2781.
[146] S.-H. Kang, J.W. Bae, K.-J. Woo, P.S.S. Prasad, K.-W. Jun, Fuel Process. Technol. 91 (2010) 399–403.
[147] V.P. Santos, T.A. Wezendonk, J.J.D. Jaen, A.I. Dugulan, M.A. Nasalevich, H.-U. Islam, A. Chojecki, S. Sartipi, X. Sun, A.A. Hakeem, A.C.J. Koeken, M. Ruitenbeek, T. Davidian, G.R. Meima, G. Sankar, F. Kapteijn, M. Makkee, J. Gascon, Nat. Commun. 6 (2015) 6451–6458.
[148] T.A. Wezendonk, V.P. Santos, M.A. Nasalevich, Q.S.E. Warringa, A.I. Dugulan, A. Chojecki, A.C.J. Koeken, M. Ruitenbeek, G. Meima, H.-U. Islam, G. Sankar, M. Makkee, F. Kapteijn, J. Gascon, ACS Catal. 6 (2016) 3236–3247.
[149] B. An, K. Cheng, C. Wang, Y. Wang, W. Lin, ACS Catal. 6 (2016) 3610–3618.
[150] B. Qiu, C. Yang, W. Guo, Y. Xu, Z. Liang, D. Ma, R. Zou, J. Mater. Chem. A 5 (2017) 8081–8086.

[151] M. Oschatz, S. Krause, N.A. Krans, C.H. Mejía, S. Kaskel, K.P. de Jong, Chem. Commun. 53 (2017) 10204–10207.
[152] S. Kattel, B. Yan, J.G. Chen, P. Liu, J. Catal. 343 (2016) 115–126.
[153] A. Goguet, F. Meunier, J.P. Breen, R. Burch, M.I. Petch, A. Faur Ghenciu, J. Catal. 226 (2004) 382–392.
[154] J.A. Rodriguez, P. Liu, D.J. Stacchiola, S.D. Senanayake, M.G. White, J.G. Chen, ACS Catal. 5 (2015) 6696–6706.
[155] X. Zhang, X. Zhu, L. Lin, S. Yao, M. Zhang, X. Liu, X. Wang, Y.-W. Li, C. Shi, D. Ma, ACS Catal. 7 (2017) 912–918.
[156] J. Zhang, B. An, Y. Hong, Y. Meng, X. Hu, C. Wang, J. Lin, W. Lin, Y. Wang, Mater. Chem. Front. 1 (2017) 2405–2409.
[157] R. Lippi, S.C. Howard, H. Barron, C.D. Easton, I.C. Madsen, L.J. Waddington, C. Vogt, M.R. Hill, C.J. Sumby, C.J. Doonan, D.F. Kennedy, J. Mater. Chem. A 5 (2017) 12990–12997.
[158] S. Wang, X. Wang, Small 11 (2015) 3097–3112.
[159] H. Zhang, G. Liu, L. Shi, H. Liu, T. Wang, J. Ye, Nano Energy 22 (2016) 149–168.
[160] C.-C. Wang, J.-R. Li, X.-L. Lv, Y.-Q. Zhang, G. Guo, Energy Environ. Sci. 7 (2014) 2831–2867.
[161] N. Salehifar, Z. Zarghami, M. Ramezani, Mater. Lett. 167 (2016) 226–229.
[162] L. He, L. Li, T. Wang, H. Gao, G. Li, X. Wu, Z. Su, C. Wang, Dalton Trans. 43 (2014) 16981–16985.
[163] P. Liang, C. Zhang, H. Sun, S. Liu, M. Tadé, S. Wang, RSC Adv. 6 (2016) 95903–95909.
[164] Z. Wu, X. Yuan, J. Zhang, H. Wang, L. Jiang, G. Zeng, ChemCatChem 9 (2017) 41–64.
[165] X. Cao, B. Zheng, X. Rui, W. Shi, Q. Yan, H. Zhang, Angew. Chem., Int. Ed. 53 (2014) 1404–1409.
[166] H. Chen, K. Shen, J. Chen, X. Chen, Y. Li, J. Mater. Chem. A 5 (2017) 9937–9945.
[167] G. Zhu, X. Li, H. Wang, L. Zhang, Catal. Commun. 88 (2017) 5–8.
[168] L. Pan, T. Muhammad, L. Ma, Z.-F. Huang, S. Wang, L. Wang, J.-J. Zou, Appl. Catal. B 189 (2016) 181–191.
[169] K.-Y.A. Lin, F.-K. Hsu, RSC Adv. 5 (2015) 50790–50800.
[170] C. Zhang, F. Ye, S. Shen, Y. Xiong, L. Su, S. Zhao, RSC Adv. 5 (2015) 8228–8235.
[171] J. Xu, J. Gao, Y. Liu, Q. Li, L. Wang, Mater. Res. Bull. 91 (2017) 1–8.
[172] Q. Xu, Z. Guo, M. Zhang, Z. Hu, Y. Qian, D. Zhao, CrystEngComm 18 (2016) 4046–4052.
[173] A. Ahmed, M. Forster, J. Jin, P. Myers, H. Zhang, ACS Appl. Mater. Interfaces 7 (2015) 18054–18063.
[174] Z. Guo, J.K. Cheng, Z. Hu, M. Zhang, Q. Xu, Z. Kang, D. Zhao, RSC Adv. 4 (2014) 34221–34225.
[175] S.J. Yang, J.H. Im, T. Kim, K. Lee, C.R. Park, J. Hazard. Mater. 186 (2011) 376–382.
[176] K.-Y.A. Lin, F.-K. Hsu, L.-W. Der, J. Mater. Chem. A 3 (2015) 9480–9490.
[177] Y.-F. Zhang, L.-G. Qiu, Y.-P. Yuan, Y.-J. Zhu, X. Jiang, J.-D. Xiao, Appl. Catal. B: Environ. 144 (2014) 863–869.
[178] K.E. deKrafft, C. Wang, W. Lin, Adv. Mater. 24 (2012) 2014–2018.
[179] Y. Li, H. Xu, S. Ouyang, J. Ye, Phys. Chem. Chem. Phys. 18 (2016) 7563–7572.
[180] Y. Su, D. Ao, H. Liu, Y. Wang, J. Mater. Chem. A 5 (2017) 8680–8689.
[181] Z.-F. Huang, J. Song, K. Li, M. Tahir, Y.-T. Wang, L. Pan, L. Wang, X. Zhang, J.-J. Zou, J. Am. Chem. Soc. 138 (2016) 1359–1365.
[182] X. Zhao, H. Yang, P. Jing, W. Shi, G. Yang, P. Cheng, Small 13 (2017) 1603279.
[183] S. Bala, I. Mondal, A. Goswami, U. Pal, R. Mondal, J. Mater. Chem. A 3 (2015) 20288–20296.
[184] J.-D. Xiao, H.-L. Jiang, Small 13 (2017) 1700632.
[185] M. Lan, R.-M. Guo, Y. Dou, J. Zhou, A. Zhou, J.-R. Li, Nano Energy 33 (2017) 238–246.
[186] M. Zhang, Y.-L. Huang, J.-W. Wang, T.-B. Lu, J. Mater. Chem. A 4 (2016) 1819–1827.
[187] Q. Lan, Z.-M. Zhang, C. Qin, X.-L. Wang, Y.-G. Li, H.-Q. Tan, E.-B. Wang, Chem. Eur. J. 22 (2016) 15513–15520.
[188] W. Tu, Y. Zhou, Z. Zou, Adv. Mater. 26 (2014) 4607–4626.
[189] H. Zhang, T. Wang, J. Wang, H. Liu, T.D. Dao, M. Li, G. Liu, X. Meng, K. Chang, L. Shi, T. Nagao, J. Ye, Adv. Mater. 28 (2016) 3703–3710.
[190] S. Wang, B. Guan, Y. Lu, X.-W. Lou, J. Am. Chem. Soc. 139 (2017) 17305–17308.
[191] J. Liu, D. Zhu, C. Guo, A. Vasileff, S.-Z. Qiao, Adv. Energy Mater. 7 (2017) 1700518.
[192] Q. Ren, H. Wang, X.-F. Lu, Y.-X. Tong, G.-R. Li, Adv. Sci. 5 (2017), https://doi.org/10.1002/advs.201700515.
[193] I.A. Khan, Y. Qian, A. Badshah, M.A. Nadeem, D. Zhao, ACS Appl. Mater. Interfaces 8 (2016) 17268–17275.
[194] H.M. Barkholtz, D.-J. Liu, Mater. Horiz. 4 (2017) 20–37.
[195] S. Ma, G.-A. Goenaga, A.V. Call, D.-J. Liu, Chem. Eur. J. 17 (2011) 2063–2067.
[196] D. Zhao, J.-L. Shui, C. Chen, X. Chen, B.M. Reprogle, D. Wang, D.-J. Liu, Chem. Sci. 3 (2012) 3200–3205.
[197] P. Zhang, F. Sun, Z. Xiang, Z. Shen, J. Yun, D. Cao, Energy Environ. Sci. 7 (2014) 442–450.
[198] B. Xia, Y. Yan, N. Li, H. Wu, X.-W. Lou, Nat. Energy 1 (2016) 15006.
[199] J. Meng, C. Niu, L. Xu, J. Li, X. Liu, X. Wang, Y. Wu, X. Xu, W. Chen, Q. Li, Z. Zhu, D. Zhao, L. Mai, J. Am. Chem. Soc. 139 (2017) 8212–8221.
[200] W. Zhang, Z.-Y. Wu, H.-L. Jiang, S.-H. Yu, J. Am. Chem. Soc. 136 (2014) 14385–14388.
[201] E. Proietti, F. Jaouen, M. Lefèvre, N. Larouche, J. Tian, J. Herranz, J.-P. Dodelet, Nat. Commun. 2 (2011) 416.
[202] P. Su, H. Xiao, J. Zhao, Y. Yao, Z. Shao, C. Li, Q. Yang, Chem. Sci. 4 (2013) 2941–2946.
[203] B. Qiao, A. Wang, X. Yang, L.F. Allard, Z. Jiang, Y. Cui, J. Liu, J. Li, T. Zhang, Nat. Chem. 3 (2011) 634–641.
[204] P. Liu, Y. Zhao, R. Qin, S. Mo, G. Chen, L. Gu, D.M. Chevier, P. Zhang, Q. Guo, D. Zang, B. Wu, G. Fu, N. Zheng, Science 352 (2016) 797–800.
[205] J. Liu, ACS Catal. 7 (2017) 34–59.
[206] X. Fang, Q. Shang, Y. Wang, L. Jiao, T. Yao, Y. Li, Q. Zhang, Y. Luo, H.-L. Jiang, Adv. Mater. 30 (2018) 1705112, https://doi.org/10.1002/adma.201705112.
[207] A. Zitolo, V. Goellner, V. Armel, M.-T. Sougrati, T. Mineva, L. Stievano, E. Fonda, F. Jaouen, Nat. Mater. 14 (2015) 937–942.
[208] P. Yin, T. Yao, Y. Wu, L. Zheng, Y. Lin, W. Liu, H. Ju, J. Zhu, X. Hong, Z. Deng, G. Zhou, S. Wei, Y. Li, Angew. Chem., Int. Ed. 55 (2016) 10800–10805.
[209] H. Zhang, S. Hwang, M. Wang, Z. Feng, S. Karakalos, L. Luo, Z. Qiao, X. Xie, C. Wang, D. Su, Y. Shao, G. Wu, J. Am. Chem. Soc. 139 (2017) 14143–14149.
[210] Y.-Z. Chen, C. Wang, Z.-Y. Wu, Y. Xiong, Q. Xu, S.-H. Yu, H.-L. Jiang, Adv. Mater. 27 (2015) 5010–5016.
[211] C. Zhang, B. An, L. Yang, B. Wu, W. Shi, Y.-C. Wang, L.-S. Long, C. Wang, W. Lin, J. Mater. Chem. A 4 (2016) 4457–4463.
[212] W. Xia, R. Zou, L. An, D. Xia, S. Guo, Energy Environ. Sci. 8 (2015) 568–576.
[213] S. Zhao, H. Yin, L. Du, L. He, K. Zhao, L. Chang, G. Yin, H. Zhao, S. Liu, Z. Tang, ACS Nano 8 (2014) 12660–12668.
[214] Y. Qian, J. Cavanaugh, I.A. Khan, X. Wang, Y. Peng, Z. Hu, Y. Wang, D. Zhao, ChemPlusChem 81 (2016) 718–723.
[215] Q. Lin, X. Bu, A. Kong, C. Mao, X. Zhao, F. Bu, P. Feng, J. Am. Chem. Soc. 137 (2015) 2235–2238.
[216] X. Fang, L. Jiao, S.-H. Yu, H.-L. Jiang, ChemSusChem 10 (2017) 3019–3024.
[217] Y. Hou, Z. Wen, S. Cui, S. Ci, S. Mao, J. Chen, Adv. Funct. Mater. 25 (2015) 872–882.
[218] Y. Xu, W. Tu, B. Zhang, S. Yin, Y. Huang, M. Kraft, R. Xu, Adv. Mater. 29 (2017) 1605957.
[219] S. Jeoung, B. Seo, J.M. Hwang, S.H. Joo, H.R. Moon, Mater. Chem. Front. 1 (2017) 973–978.
[220] H. Tabassum, W. Guo, W. Meng, A. Mahmood, R. Zhao, Q. Wang, R. Zou, Adv. Energy Mater. 7 (2017) 1601671.
[221] Y.-J. Tang, M.-R. Gao, C.-H. Liu, S.-L. Li, H.-L. Jiang, Y.-Q. Lan, M. Han, S.-H. Yu, Angew. Chem., Int. Ed. 54 (2015) 12928–12932.
[222] L. Fan, P. Liu, X. Yan, L. Gu, Z. Yang, H. Yang, S. Qiu, X. Yao, Nat. Commun. 7 (2016) 10667.
[223] P. He, X.-Y. Yu, X.-W. Lou, Angew. Chem., Int. Ed. 56 (2017) 3897–3900.
[224] X. Fang, L. Jiao, R. Zhang, H.-L. Jiang, ACS Appl. Mater. Interfaces 9 (2017) 23852–23858.
[225] K. Jayaramulu, J. Masa, O. Tomanec, D. Peeters, V. Ranc, A. Schneemann, R. Zboril, W. Schuhmann, R.A. Fischer, Adv. Funct. Mater. 27 (2017) 1700451.
[226] Y. Guo, J. Tang, H. Qian, Z. Wang, Y. Yamauchi, Chem. Mater. 29 (2017) 5566–5573.
[227] X.-F. Lu, L.-F. Gu, J.-W. Wang, J.-X. Wu, P.-Q. Liao, G.-R. Li, Adv. Mater. 29 (2017) 1604437.
[228] K.J. Lee, Y.J. Sa, H.Y. Jeong, C.W. Bielawski, S.H. Joo, H.R. Moon, Chem. Commun. 51 (2015) 6773–6776.
[229] Y. Qian, Z. Hu, X. Ge, S. Yang, Y. Peng, Z. Kang, Z. Liu, J.Y. Lee, D. Zhao, Carbon 111 (2017) 641–650.
[230] S. Liu, Z. Wang, S. Zhou, F. Yu, M. Yu, C.-Y. Chiang, W. Zhou, J. Zhao, J. Qiu, Adv. Mater. 29 (2017) 1700874.
[231] C. Guan, X. Liu, A.M. Elshahawy, H. Zhang, H. Wu, S.J. Pennycook, J. Wang, Nanoscale Horiz. 2 (2017) 342–348.
[232] J. Li, Q.-L. Zhu, Q. Xu, Chem. Commun. 51 (2015) 10827–10830.
[233] C. Zhao, X. Dai, T. Yao, W. Chen, X. Wang, J. Wang, J. Yang, S. Wei, Y. Wu, Y. Li, J. Am. Chem. Soc. 139 (2017) 8078–8081.
[234] X. Sun, Q. Zhu, J. Hu, X. Kang, J. Ma, H. Liu, B. Han, Chem. Sci. 8 (2017) 5669–5674.
[235] Y. Liu, Y. Su, X. Quan, X. Fan, S. Chen, H. Yu, H. Zhao, Y. Zhang, J. Zhao, ACS Catal. 8 (2018) 1186–1191.